A wake oscillator model with nonlinear coupling for the vortex-induced vibration of a rigid cylinder constrained to vibrate in the cross-flow direction

Qu, Yang; Metrikine, Andrei V.

DOI
10.1016/j.jsv.2019.115161

Publication date
2020

Document Version
Accepted author manuscript

Published in
Journal of Sound and Vibration

A wake oscillator model with nonlinear coupling for the vortex-induced vibration of a rigid cylinder constrained to vibrate in the cross-flow direction

Yang Qu[a,b,*], Andrei V. Metrikine[b,c]

[a] *State Key Laboratory of Ocean Engineering, Shanghai Jiao Tong University, Shanghai, 200240, China*
[b] *Department of Hydraulic Engineering, Delft University of Technology, Stevinweg 1, 2628CN Delft, The Netherlands*
[c] *Department of Engineering Structures, Delft University of Technology, Stevinweg 1, 2628CN Delft, The Netherlands*

Abstract

In this paper, a new wake oscillator model with nonlinear coupling is proposed for the modelling of vortex-induced vibration. The purpose is to develop a model that is capable of reproducing both free and forced vibration experiments. To achieve this goal, an existing van der Pol wake oscillator model is first reviewed. The limitations of the model are discussed and the influence of different drag force models on the dynamic characteristics of the fluctuating lift force that matches the forced vibration experiments are studied. Based on this model, nonlinear coupling terms are introduced to improve its predictive capabilities. The tuning of this improved model to the forced vibration shows a good agreement with experiments in terms of the added damping. However, the model failed to capture the negative added mass at high reduced velocities. As a result, the new model underpredicts both the range and frequency of lock-in in free vibration tests. To eliminate this discrepancy, the model is further enhanced by introducing frequency dependent nonlinear couplings, which are achieved in the time domain by means of convolution integrals. A single set of frequency dependent, complex-valued functions – which are the Laplace transforms of corresponding convolution kernels – that reproduce the forced vibration experiments is determined over a limited range of frequencies. However, no analytical extension of these functions to the infinite frequency domain was found such that the causality principle and the energy conservation would be satisfied. The latter is a major challenge for all existing wake oscillator models that aim at reproducing the forced vibration experiments.

Keywords: cross-flow vortex-induced vibration, wake oscillator model, forced vibration, nonlinear coupling

1. Introduction

As fluid flows around a cylinder, due to the fluid viscosity, a boundary layer will be formed, and the flow will separate from the cylinder, resulting in vortex shedding downstream of the cylinder. The alternate shedding of vortices in the near wake gives rise to a fluctuating cross-flow force

*Corresponding author
Email address: yangqu@sjtu.edu.cn (Yang Qu)

on the cylinder. In the cases where the cylinder is free to move, the fluctuating hydrodynamic force can result in self-excited oscillation of the cylinder. Experiments have demonstrated that for an elastically-mounted rigid cylinder, the vibration of the cylinder reaches maximum when the vortex shedding frequency approaches the natural frequency of the system. Within a certain range of flow velocities that brackets the natural frequency of the system, the vortex shedding frequency will deviate from the Strouhal relation and collapse onto the oscillation frequency of the cylinder, resulting in the sustained vibration of the cylinder over a wide range of flow velocities. This phenomenon is termed as vortex-induced vibration (VIV).

VIV is a well-known phenomenon to offshore engineers, due to the fact that cylindrical structures such as risers, offshore pipelines and mooring cables are frequently used in offshore facilities. When subjected to cross flow currents these structures will undergo VIVs. Since this type of vibration will significantly reduce the service life of the structure, the prediction of VIV has been one of the key issues in the analysis and design of offshore structures.

Driven by the demand from the oil and gas industry, VIV has been extensively studied in the past century to develop a prediction tool that can be applied in the design of offshore structures. Due to the complexity of the fluid-structure interaction problem, most knowledge about VIV to date has been obtained from physical experiments. It is the VIV of rigid cylinders that has been the focus of early research. Two types of experiments have been adopted by the majority of researchers to investigate the problem: free and forced vibration tests. In the free vibration tests an elastically supported rigid cylinder vibrates due to the fluid-structure interaction, and the characteristics of the motion are analysed. The forced vibration test, on the other hand, investigates the hydrodynamic forces acting on and the wake structure behind a cylinder that is forced to vibrate with constant amplitude and frequency. Reviews of these studies can be found in the papers by Williamson and Govardhan [1] and Sarpkaya [2].

Based on the understanding of the problem from experiments, several semi-empirical approaches for the prediction of VIV, such as force-decomposition methods, wake oscillator models, single degree-of-freedom models and approach based on variational principles have been developed. A Detailed review of these models can be found in Ref.[3]. In particular, the wake oscillator model has been the focus of many works in recent years. The fundamental idea of this approach is to describe the dynamics of the wake using an effective nonlinear oscillator, whose motion is coupled to the dynamics of the cylinder. Instead of modelling the real flow field, this model attempts to reproduce the main features of VIV observed in cross-flow only and coupled cross-flow and in-line free vibration tests [4–11], and it is thus phenomenological. Although the wake oscillator model qualitatively captures the main characteristics of VIV, applying it in the prediction of VIV requires it to reproduce the experiments more quantitatively. In fact this has been the focus of several recent studies where much effort has been placed on the modification of classic wake oscillator models such that a better quantitative reproduction of the results from free vibration experiments, cross-flow only or coupled cross-flow and in-line vibrations, of elastically supported rigid cylinders can be achieved [12–14]. Attention has also been paid to the development of a wake oscillator model that can reproduce the forced vibration experiments [15], which, in the authors' opinion, is of high importance. In contrast to the free vibration experiments, the forced vibration experiments, in which a certain amplitude and frequency of the harmonic motion of a cylinder is maintained, provide additional insights into the interaction mode between the hydrodynamic force and the cylinder motion. Only with the reproduction of both the free and forced vibration experiments can the wake oscillator model be classified as a useful one, as it will contain correct nonlinearities that describe the interaction between the flow and structure.

The objective of this paper is to develop a wake oscillator model that is capable of reproducing

both the free and forced vibration experiments when the motion of the cylinder is constrained to the cross-flow direction. The paper starts with the description and review of the model proposed by Ogink and Metrikine [15] in Section 2, which is the first paper in which an attempt was made to develop a wake oscillator model that complies both the forced and free vibration experiments. The review is ammended by an analysis of the influence of different drag force models on the dynamic characteristic of the fluctuating lift force that satisfies the forced vibration tests. In Section 3, a new wake oscillator model with nonlinear coupling is proposed and its capability of reproducing the experiments are examined. Thereafter, the model is further enhanced by introducing frequency dependent coupling in Section 4. Finally, in Section 5 concluding remarks are given.

2. Wake oscillator model by Ogink and Metrikine

Ogink and Metrikine [15] are the first authors who attempted to develop a wake oscillator model that is able to reproduce both the free and forced vibration experiments. In their work, they tried to formulate the total hydrodynamic force as a summation of the ideal inviscid inertia force and a 'vortex force'. This is a common approach adopted by most wake oscillator models. The main novelty of their work lies in the formulation of the vortex force. Different from other models where only the component of the vortex force in the cross-flow direction is considered, the vortex force in their model is formulated as a vector normal to the cylinder axis and is decomposed into instantaneous lift and drag forces. The quasi-steady assumption is adopted regarding the drag force, while the influence of the wake dynamics is taken into account by relating the lift force to a wake oscillator that is coupled with the motion of the structure. According to the quasi-steady assumption, the data measured in the static (fixed cylinder) situation can be directly applied in the description of the dynamics of the interaction between a structure and fluid [16]. The advantage of this force decomposition is threefold: (a) it provides the possibility of not only modelling the cross-flow hydrodynamic force but also the in-line force, and the influence of the wake dynamics on both forces have been accounted for through the lift force; (b) the assumption of a linearized stall term that has been taken in previous wake oscillator models is relaxed, and the authors found that the free vibration experiments can be better reproduced if the nonlinear stall effect is considered; and (c) when the cylinder oscillates in the still fluid, this force decomposition results in the hydrodynamic force given by the Morison equation.

Despite all of the advantages described above, there are also several problems related to this force decomposition that need to be investigated. One of them is the quasi-steady assumption of the drag force. This assumption is physically incorrect, and whether it provides a reasonable approximation or if another drag force model is required should be studied.

2.1. Model Description

This section contains a recollection of the wake oscillator model proposed by Ogink and Metrikine [15]. The purpose is to provide a general and critical review of the model.

Fig. 1 illustrates the VIV of a rigid cylinder elastically supported in the cross-flow direction. The cylinder has mass m, and its motion is constrained to the cross-flow direction only where it is supported by a spring with stiffness k and dash pot with damping b. The cross-flow displacement of the cylinder $Y(t)$ is governed by the following ODE:

$$m\frac{d^2Y}{dt^2} + b\frac{dY}{dt} + kY = F_Y \tag{1}$$

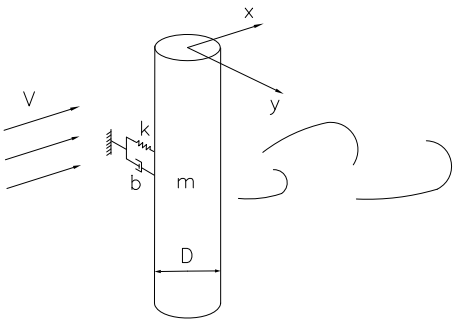

Figure 1: Cross-flow VIV of an elastically supported rigid cylinder subjects to uniform flow.

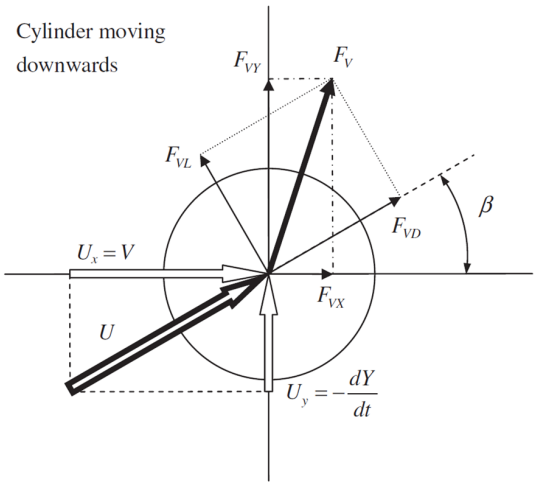

Figure 2: Decomposition of the vortex force in drag, lift, cross-flow and in-line directions [15].

On the right-hand side of Eq. (1), F_Y is the cross-flow hydrodynamic force acting on the cylinder. This force is assumed to be expressible as a superposition of a vortex force F_{VY} and an ideal inviscid inertia force F_{AY} associated with the potential added mass of the fluid:

$$F_Y = F_{VY} + F_{AY} = \frac{1}{2}\rho DLV^2 C_{VY} - m_a \frac{d^2Y}{dt^2} \tag{2}$$

where ρ is the mass density of the fluid; D is the diameter; L is the length of the cylinder; C_{VY} is the cross-flow vortex force coefficient; $m_a = C_a \pi \rho D^2 L/4$ is the ideal added mass; and the value for C_a is 1, as follows from the potential theory. Moving the potential inertia term to the left-hand side of Eq.(1) and defining the structural natural frequency in still water $\omega_n = \sqrt{k/(m+m_a)}$ and damping ratio $\zeta = b/\left(2\sqrt{(m+m_a)\,k}\right)$, Eq.(1) becomes

$$\frac{d^2Y}{dt^2} + 2\zeta\omega_n \frac{dY}{dt} + \omega_n^2 Y = \frac{F_{VY}}{m+m_a} \tag{3}$$

Note here that F_{VY} corresponds to the cross-flow component of the total instantaneous vortex force F_V caused by vorticity, which includes the effect of stall. In other studies, such as those by Facchinetti et al. [8] and Skop and Balasubramanian [17], the stall effect has been normally taken into account by adding a constant linear damping term at the left-hand side of the structural equation Eq.(1), and the damping coefficient related to the stall is determined by assuming that the cylinder velocity is much smaller than the flow velocity V. This assumption has been relaxed in the model proposed by Ogink and Metrikine [15], where the total instantaneous vortex force F_V is decomposed into a drag part F_{VD} and a lift part F_{VL}, both of which are illustrated in Fig.2. As can be seen from this figure, the drag force F_{VD}, defined as being in-line with the relative flow velocity $U = \sqrt{V^2 + \left(\frac{dY}{dt}\right)^2}$, models the stall effect, and the lift force F_{VL} that acts in the direction perpendicular to the U formulates the excitation by vortex shedding. The magnitudes of drag and lift forces are related to the relative flow velocity U and are defined as

$$F_{VL} = \frac{1}{2}\rho DLU^2 C_{VL}, F_{VD} = \frac{1}{2}\rho DLU^2 C_{VD} \tag{4}$$

where C_{VL} and C_{VD} are lift and drag coefficients. The effects of the wake dynamics are taken into account by the lift coefficient C_{VL} (with the wake variable that is governed by the wake oscillator, to be discussed later).

Then, the cross-flow component F_{VY} of the vortex force is the summation of projections of F_{VL} and F_{VD} in the cross-flow direction, and it can be written as

$$F_{VY} = F_{VD}\sin\beta + F_{VL}\cos\beta \tag{5}$$

where β is the angle between the direction of relative flow velocity U and the undisturbed flow velocity V. The angle β is given by

$$\sin\beta = -\frac{dY}{dt}\left(V^2 + \left(\frac{dY}{dt}\right)^2\right)^{-1/2} \quad \text{or} \quad \cos\beta = V\left(V^2 + \left(\frac{dY}{dt}\right)^2\right)^{-1/2} \tag{6}$$

Substitution of Eqs.(4) and (6) into Eq. (5) results in

$$F_{VY} = \frac{1}{2}\rho DL\left(-C_{VD}\frac{dY}{dt} + C_{VL}V\right)\sqrt{V^2 + \left(\frac{dY}{dt}\right)^2} \tag{7}$$

Furthermore, the corresponding force coefficient C_{VY} can be obtained as

$$C_{VY} = \frac{F_{VY}}{\frac{1}{2}\rho DLV^2} = \left(-C_{VD}\frac{dY}{dt}/V + C_{VL}\right)\sqrt{1 + \left(\frac{dY}{dt}/V\right)^2} \tag{8}$$

Similarly, the in-line component F_{VX} of the vortex force and coefficient C_{VX} can be expressed as

$$F_{VX} = F_{VD}\cos\beta - F_{VL}\sin\beta = \frac{1}{2}\rho DL\left(C_{VD}V + C_{VL}\frac{dY}{dt}\right)\sqrt{V^2 + \left(\frac{dY}{dt}\right)^2} \tag{9}$$

$$C_{VX} = \frac{F_{VX}}{\frac{1}{2}\rho DLV^2} = \left(C_{VD} + C_{VL}\frac{dY}{dt}/V\right)\sqrt{1 + \left(\frac{dY}{dt}/V\right)^2} \tag{10}$$

The final expression of the total cross-flow hydrodynamic force is obtained by substituting Eq.(7) into Eq.(2)

$$F_Y = \frac{1}{2}\rho DL\left(-C_{VD}\frac{dY}{dt} + C_{VL}V\right)\sqrt{V^2 + \left(\frac{dY}{dt}\right)^2} - m_a\frac{d^2Y}{dt^2} \tag{11}$$

As presented in Ref.[15], by setting $V = 0$ Eq.(11) transforms into

$$F_Y = -\frac{1}{2}\rho DLC_{VD}\frac{dY}{dt}\left|\frac{dY}{dt}\right| - m_a\frac{d^2Y}{dt^2} \tag{12}$$

which is the Morison equation.

The wake oscillator that describes the fluctuating nature of the vortex is based on the van der Pol equation that reads

$$\frac{d^2q}{dt^2} + \epsilon\omega_s(q^2 - 1)\frac{dq}{dt} + \omega_s^2 q = S \tag{13}$$

where ϵ is the tuning paramter, and ω_s is the Strouhal frequency, $\omega_s = \mathrm{St}V/(2\pi D)$. The forcing term S on the right-hand side models the effects of the cylinder motion on the wake. The dimensionless wake variable q is associated with the lift force coefficient C_{VL} as

$$C_{VL} = \frac{q}{2}C_{L0} \tag{14}$$

where C_{L0} is the lift coefficient measured on a fixed cylinder subjected to vortex shedding, and the coefficient 1/2 is used to ensure the amplitude of oscillation of C_{VL} equals to C_{L0} for a fixed cylinder ($S = 0$).

The usage of the van der Pol type oscillator in Eq.(13) is based on the similar characteristics between the vortex-shedding process and self-limitation and self-excitation of nonlinear oscillators. Any nonlinear oscillator that generates a limit cycle can potentially be used to represent the vortex-shedding process. However, the most commonly used nonlinear oscillators are the van der Pol and the Rayleigh equations or a combination of both. The Rayleigh equation is similar to the van der Pol equation except for the nonlinear damping term, which reads $((\frac{dq}{dt})^2 - 1)\frac{dq}{dt}$.

With regard to the forcing term on the right-hand side of Eq.(13), Facchinetti et al. [8] have proven that a linear coupling – with respect to the acceleration of the cylinder – models most of the important features of the VIV qualitatively. In the model proposed by Ogink and Metrikine [15], both acceleration and velocity couplings are used:

$$S = \frac{A}{D}\frac{dY^2}{dt^2} + \omega_s\frac{B}{D}\frac{dY}{dt} \tag{15}$$

where A and B are coupling coefficients, which can be tuned to meet the experimental results.

The problem can be made dimensionless using the following dimensionless parameters:

$$\tau = \omega_s t, \Omega_n = \omega_n/\omega_s, y = Y/D. \tag{16}$$

Substitution of Eq.(16) into Eqs.(3), (13) and (15) results in

$$\ddot{y} + 2\zeta\Omega_n\dot{y} + \Omega_n^2 y = \frac{1}{\pi(m^* + C_a)}\frac{1}{2\pi^3\mathrm{St}^2}C_{VY} \tag{17}$$

$$\ddot{q} + \epsilon(q^2 - 1)\dot{q} + q = s \tag{18}$$

$$s = A\ddot{y} + B\dot{y} \tag{19}$$

The dimensionless forms of C_{VX} and C_{VY} can be obtained by substituting Eq.(16) into Eqs.(8) and (10), and they read

$$C_{VX} = (C_{VD} + 2\pi \mathrm{St}\dot{y} C_{VL}) \sqrt{1 + 4\pi^2 \mathrm{St}^2 \dot{y}^2} \tag{20}$$

$$C_{VY} = (-2\pi \mathrm{St}\dot{y} C_{VD} + C_{VL}) \sqrt{1 + 4\pi^2 \mathrm{St}^2 \dot{y}^2} \tag{21}$$

In above equations, the overdot stands for the derivative with respect to the dimensionless time τ, and $m^* = \frac{m}{\frac{1}{4}\rho\pi LD^2}$ is the mass ratio.

The coupled system described by Eqs.(17-19) and (21) governs the VIV of rigid cylinders in the cross-flow direction. This system can be used in the simulation of cross-flow free vibrations of rigid cylinders at different nominal reduced velocities V_n. The definition of V_n is given as $V_n = \frac{2\pi V}{\omega_n D}$ which can also be expressed with dimensionless parameters as $V_n = \frac{1}{\mathrm{St}\Omega_n}$.

For the forced vibration, the motion of the cylinder is prescribed with a dimensionless frequency $\Omega = \omega/\omega_s$ (ω is the dimensional frequency of the cross-flow motion of the cylinder) and a dimensionless amplitude y_0. This motion is given as $y = y_0 \sin(\Omega\tau)$. The results of forced vibration are normally presented against the true reduced velocity $V_r = \frac{2\pi V}{\omega D}$, which can be alternatively written using the dimensionless parameters as $V_r = \frac{1}{\mathrm{St}\Omega}$. The forced vibration can be modelled by substituting $y = y_0 \sin(\Omega\tau)$ into Eqs.(18) and (19), which then gives

$$\ddot{q} + \epsilon(q^2 - 1)\dot{q} + q = s \tag{22}$$

$$s = -Ay_0\Omega^2 \sin(\Omega\tau) + By_0\Omega \cos(\Omega\tau) \tag{23}$$

The cross-flow force coefficient $C_y = \frac{F_Y}{\frac{1}{2}\rho DLV^2}$ can be calculated from Eq. (11), and its dimensionless form is given as

$$C_y = (-2\pi \mathrm{St}\dot{y} C_{VD} + C_{VL}) \sqrt{1 + 4\pi^2 \mathrm{St}^2 \dot{y}^2} - 2C_a\pi^3 \mathrm{St}^2 \ddot{y} \tag{24}$$

Since the cylinder does not move in the in-line direction, the in-line force coefficient C_x is equal to C_{VX} and is given as

$$C_x = C_{VX} = (C_{VD} + 2\pi \mathrm{St}\dot{y} C_{VL}) \sqrt{1 + 4\pi^2 \mathrm{St}^2 \dot{y}^2} \tag{25}$$

Then, the component of the cross-flow force coefficient that is in phase with cylinder acceleration C_{ya} and in phase with cylinder velocity C_{yv}, the mean in-line force coefficient C_{x0} and the magnitude of fluctuating in-line force coefficient C_{x2} can be obtained through the Fourier series:

$$C_{ya} = \frac{2}{T} \int_{\tau_0}^{\tau_0+T} C_y \sin(\Omega\tau)\, d\tau \tag{26}$$

$$C_{yv} = -\frac{2}{T} \int_{\tau_0}^{\tau_0+T} C_y \cos(\Omega\tau)\, d\tau \tag{27}$$

$$C_{x0} = \frac{1}{T}\int_{\tau_0}^{\tau_0+T} C_x d\tau \tag{28}$$

$$C_{x2} = \left(\left(\frac{2}{T}\int_{\tau_0}^{\tau_0+T} C_x \sin(2\Omega\tau)\, d\tau\right)^2 + \left(\frac{2}{T}\int_{\tau_0}^{\tau_0+T} C_x \cos(2\Omega\tau)\, d\tau\right)^2\right)^{\frac{1}{2}} \tag{29}$$

where $T = 2\pi/\Omega$ is the non-dimensional period of the forced oscillation. It needs to be noticed here that the definition of C_{yv} given by Eq.(27) is such that a negative value of C_{yv} corresponds to the case of energy supply from the flow into the structure.

2.2. Limitations of the drag force model proposed by Ogink and Metrikine

It is clear from previous subsection that the proper representation of the total hydrodynamic force requires the correct modelling of both lift and drag forces. Efforts have been made by Ogink and Metrikine [15] to improve the lift force model in order to reproduce the experimental measurements. However, little is known yet about whether the drag force model adopted by Ogink and Metrikine [15] is appropriate. Trying to reproduce the experimental measurements, with a drag force model that is likely to be deficient, by improving the modelling of the lift force may be difficult, if not impossible, as the lift force model needs to compensate for the errors introduced by the drag force model.

The drag force model proposed by Ogink and Metrikine [15] adopts the quasi-steady assumption, which assumes that the instantaneous drag force acting on an oscillating cylinder keeps its stationary value, while the change in the dynamics of the wake is taken into account through the instantaneous lift force that is coupled with the cylinder motion. The quasi-steady assumption regarding the drag force is physically not fully appropriate, as it ignores the time that the wake needs to develop. Due to the viscosity, when the position of the cylinder changes, the wake behind it cannot immediately reach its steady-state configuration, and the drag force thus no longer keeps its steady value. Moreover, for the sake of simplification, only the mean value of the steady drag force has been adopted in the model by Ogink and Metrikine [15]. This is mainly because its oscillatory part, which should be coupled with the lift, at double the frequency of vortex shedding, is small and normally ignored. However, due to the increase in the correlation length of vortex shedding and the strength of vortices when the cylinder moves, the oscillatory component of the drag force may become non-negligible. More importantly, this fluctuating force may contain crucial information regarding the wake dynamics and can play an important role in the formulation of hydrodynamic forces. Another drawback related to the current drag force model is that it neglects the added mass introduced by the dynamics of the wake in the direction parallel to the instantaneous flow velocity. The limitations of the model as a result of ignoring such an inertial component can be emphasised by the case of a rigid cylinder oscillating in still water. In such a case, according to Eq.(12), the current model is reduced to the well-known Morison equation with a fixed value of inviscid added mass coefficient. This is contradictory to the experimental measurements, which show that the added mass coefficient deviates from its inviscid value and strongly depends on the amplitude and frequency of cylinder oscillation [18].

To summarise, the main shortcomings of the drag force model is threefold: (a) making a quasi-steady assumption, (b) ignoring the oscillatory component, and (c) neglecting the inertia force introduced by the dynamics of the wake in the direction of the drag force. In this section, the influence of the first two drawbacks on the modelling of the lift force is investigated, while the third one is not studied.

The investigation is based on three drag force models, which are given as

$$C_{VD} = C_{D0} \tag{30}$$

$$C_{VD} = C_{D0}\left(\Omega, y_0\right) \tag{31}$$

$$C_{VD} = C_{D0}\left(\Omega, y_0\right) + \alpha\left(\Omega, y_0\right) C_{VL}^2 \tag{32}$$

The first drag force model, Eq.(30), is the same one as proposed by Ogink and Metrikine [15], where the drag force coefficient is assumed to be constant and to maintain the steady mean value that is measured on a fixed cylinder. In the second drag force model, given by Eq.(31), the quasi-steady assumption is relaxed to some extent by making the drag force coefficient frequency- and amplitude-dependent. The third model, Eq.(32), in addition to the mean drag force coefficient, contains an oscillatory component, which is coupled to the lift force in the same form as derived from the fixed cylinder [19]. It needs to be pointed out that introducing only the frequency-dependent drag coefficient is not correct, as such frequency-dependent damping should always be accompanied by a frequency-varying inertial component. However, only the frequency-dependent damping is considered here in order to understand what the frequency dependence of the drag coefficient could be if the frequency dependence of the inertial component in the frequency band of interest were weak.

2.3. Determination of the lift force that conforms to the experiments

In this subsection, the lift force that matches the experimental measurements is determined based on the drag force models proposed in the previous subsection. So far, the most complete, publicly available forced vibration measurements are reported by Gopalkrishnan [20]. In this work, the component of cross-flow force coefficient in phase with the cylinder acceleration C_{ya} and that in phase with the cylinder velocity C_{yv}, the mean in-line force coefficient C_{x0} and the amplitude of the oscillatory in-line force coefficient C_{x2} are reported. Among these four types of measurements, C_{ya} and C_{yv} are of the main interest, as they govern the cross-flow response of the structure in free vibration. The other two measurements regarding the force in the in-line direction would play important roles when the cylinder is also allowed to move in that direction. The ideal scenario would be that all four measurements can be reproduced by one and the same model for the hydrodynamic force. However, this may be impossible for the drag force models proposed here. Therefore, the priority of this work is to reproduce the measurements of C_{ya} and C_{yv}.

As for the oscillatory lift force C_{VL}, although it may physically contain multiple frequency components, the assumption here is that mainly the part at the frequency of cylinder oscillation contributes to C_{ya} and C_{yv}. This assumption, strictly speaking, is discussible, as the other harmonics at an integer multiple frequency of cylinder motion must have an influence on the results. Since no experimental measurement is available at those frequencies, it is difficult to evaluate whether their influences are significant or negligible. This leaves no better option than to neglect the influence of higher harmonics and to assume that the oscillatory lift force has the form $C_{VL} = C_{VL0}\sin\left(\Omega\tau + \phi_{VL}\right)$. C_{VL0} represents the amplitude of the lift force coefficient, while ϕ_{VL} designates the phase difference between the lift force and cylinder motion $y = y_0\sin\left(\Omega\tau\right)$.

For the first drag force model, by substituting $C_{VL} = C_{VL0}\sin\left(\Omega\tau + \phi_{VL}\right)$ and $y = y_0\sin\left(\Omega\tau\right)$ into Eqs.(21), (26), (27), (28) and (29) and applying the numerical integration, the fluid force coefficient C_{ya} and C_{yv} can be obtained with a given C_{VL0} and ϕ_{VL}. The values of C_{VL0} and ϕ_{VL}

that satisfy the experimental measurements are identified by minimising the error between the calculations and measurements:

$$\text{error} = \left(C_{ya;model} - C_{ya;meaured}\right)^2 + \left(C_{yv;model} - C_{yv;meaured}\right)^2 \tag{33}$$

The value of C_{D0} needs to be specified in advance; here, the value $C_{D0} = 1.1856$ is taken as measured on the fixed cylinder. A Matlab built-in function 'lsqnonlin' has been used for the minimisation procedure, and the values of C_{VL0} and ϕ_{VL} are obtained at each frequency and amplitude of cylinder oscillation with an error smaller than 10^{-6}. The results are plotted in Fig.3.

From Fig.3 it can be seen that the dynamic characteristics of the lift force coefficient, regarding its amplitude and phase, change as the amplitude of cylinder oscillation increases. Three different patterns are generally observed, and they can be categorised as a small amplitude pattern ($y_0 = 0.2, 0.4$), a medium amplitude pattern ($y_0 = 0.6, 0.8, 1.0$) and a large amplitude pattern ($y_0 = 1.2$). When the cylinder oscillates at small amplitudes – $y_0 = 0.2$ and 0.4 – then the frequency dependence of the amplitude and phase of the lift force, although not exact, is in good agreement with the phenomenon of resonance; i.e. the amplitude peak is accompanied by a sharp change of the phase. For $y_0 = 0.2$, as depicted in plot (a) in Fig.3, the phase of the lift force remains constant at small frequencies and changes around $\Omega = 0.9$ from 0.8π to just below 0. When the cylinder oscillates at $y_0 = 0.4$, the resonance is less obvious than in the case of $y_0 = 0.2$; however, a peak in the amplitude is still observed and is accompanied by a phase change around $\Omega = 0.9$. It must be pointed out that the amplitude of the lift force in the case of $y_0 = 0.4$ is not double of that at $y_0 = 0.2$. When the cylinder oscillates at medium amplitudes, i.e. $y_0 = 0.6, 0.8$ and 1.0, the phase change is observed around $\Omega = 0.9$. However, instead of a peak in the amplitude, which is seen when the cylinder oscillates at small amplitudes, the phase change is accompanied by a local minimum in amplitude, and the trough becomes deeper as the amplitude of cylinder oscillation increases. Finally, when the cylinder oscillates at a large amplitude ($y_0 = 1.2$), the phase of the lift force is again characterised by a sharp change around $\Omega = 1$. However, different from the small and medium amplitude patterns, the phase change is associated with neither a peak nor a trough of the amplitude-frequency dependence. It seems that after the amplitude of the lift force reaches a minimum, instead of increasing, as observed in the case of a medium amplitude pattern, it maintains relatively small values at high frequencies. In general, the lift force determined from the first drag force model follows the resonance pattern at small amplitudes of cylinder motion, whereas at medium and large amplitudes of cylinder motion, its pattern is not consistent with the dependence typical for the resonance phenomenon.

With the obtained lift force, the values of C_{x0} and C_{x2} are calculated based on the first drag force model, and the results are depicted in Fig.4 in comparison with the experimental results. Fig.4(a) illustrates that the calculated mean in-line force coefficients C_{x0} are in qualitative agreement with the measurements. The increasing trend of the mean in-line force coefficients with respect to the increasing frequency is well captured. However, over the range of $\Omega = 0.7 - 1.2$, where VIV usually occurs, the first model generally underestimates the mean in-line force. As for the oscillatory in-line force, Fig.4(b) demonstrates good agreement between the results of the model and the measurements over the range of low frequencies, but at high frequencies, the model significantly underestimates C_{x2} for amplitudes of cylinder oscillation larger than 0.2. It is interesting to notice that the discrepancy starts to emerge around $\Omega = 1.0$, which is the point at which the frequency of cylinder oscillation equals the Strouhal frequency and corresponds to a wake change between the 2P mode and the 2S mode [21].

For the second drag force model, since one extra coefficient $C_{D0}(\Omega, y_0)$ needs to be identified, the reproduction of the measurement of C_{x0} is also considered in the minimisation procedure,

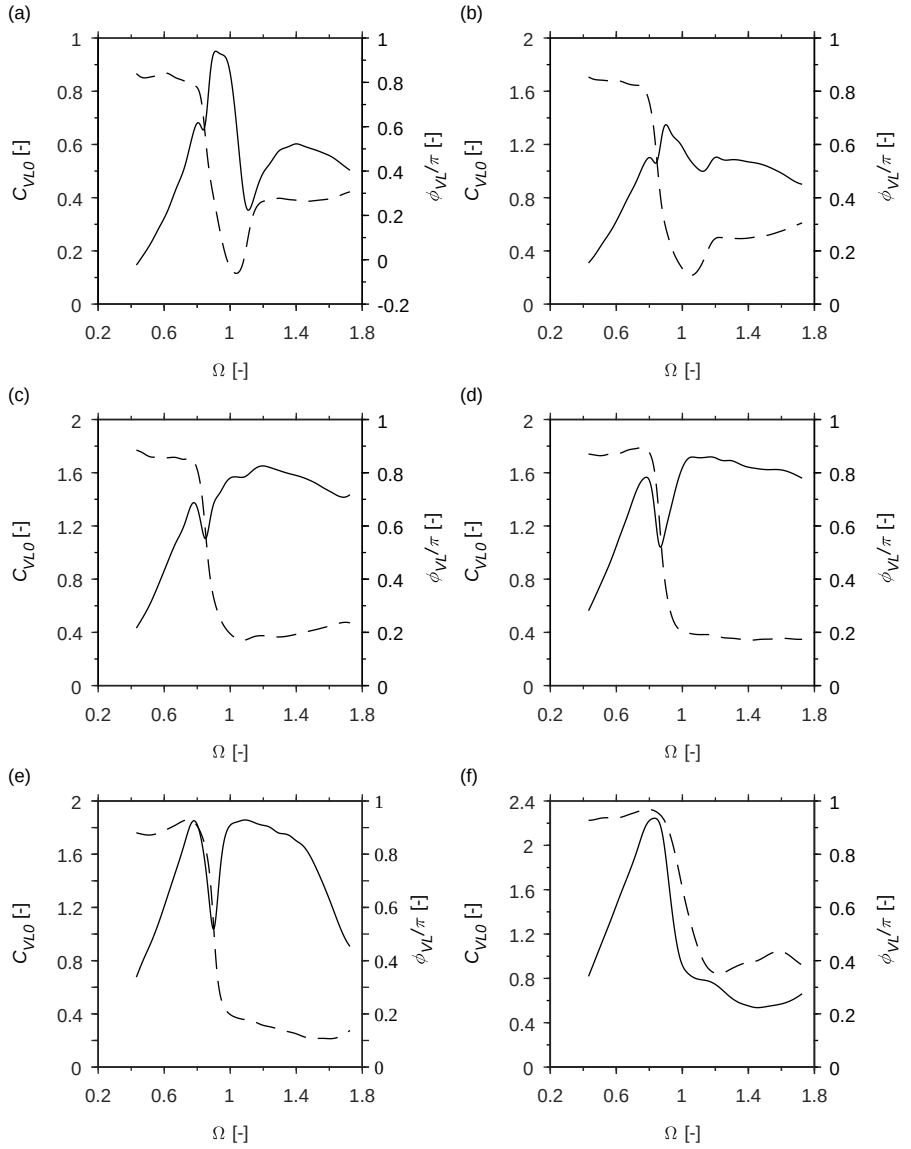

Figure 3: Amplitudes (solid lines) and phases (dashed lines) of the oscillatory lift force coefficient that conforms to the forced vibration measurements with first drag force model at different amplitudes of cylinder oscillation (a) $y_0 = 0.2$, (b) $y_0 = 0.4$, (c) $y_0 = 0.6$, (d) $y_0 = 0.8$, (e) $y_0 = 1.0$ and (f) $y_0 = 1.2$.

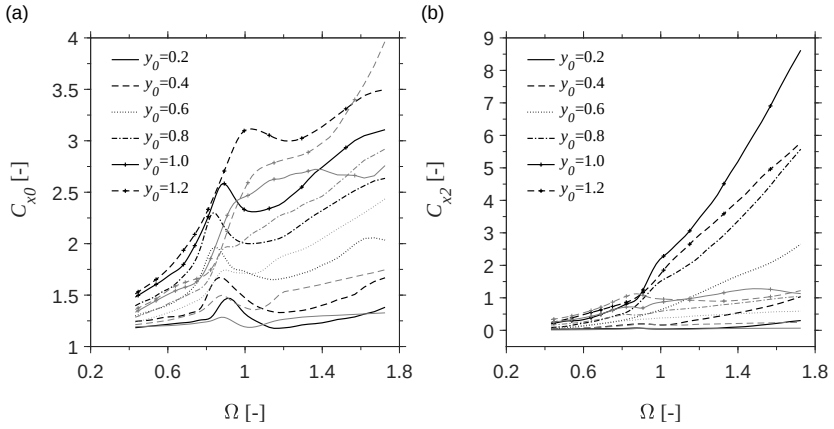

Figure 4: Force coefficients obtained from the first drag force model (gray thin lines) in comparison with the measurements (black thick lines) for (a) mean in-line force coefficient C_{x0} and (b) oscillatory in-line force coefficient C_{x2}.

and the definition of error becomes

$$\text{error} = \left(C_{ya;model} - C_{ya;meaured}\right)^2 + \left(C_{yv;model} - C_{yv;meaured}\right)^2 + \left(C_{x0;model} - C_{x0;meaured}\right)^2 \quad (34)$$

Applying the same minimisation routine, the values of C_{VL0}, ϕ_{VL} and $C_{D0}(\Omega, y_0)$ that meet the experimental results based on the second drag force model have been determined. It was found that the values of C_{VL0} and ϕ_{VL} are almost the same as those calculated with the first drag force model. Therefore, the results of C_{VL0} and ϕ_{VL} are not presented here, and only the frequency- and amplitude-dependent $C_{D0}(\Omega, y_0)$ are depicted in Fig.5. At all amplitudes, the variation of the $C_{D0}(\Omega, y_0)$ against frequency follows a similar pattern, which exhibits a local peak around $\Omega = 0.9$. No general trend is observed regarding the variation of $C_{D0}(\Omega, y_0)$ with respect to the amplitude. The values of C_{x2} are also calculated for the second drag force model with the obtained oscillatory lift force coefficient. However, no obvious difference is found compared to those calculated from the first model, and the results are thus not presented here.

The third drag force model, in addition to the frequency- and amplitude-dependent drag force coefficient, takes into account the oscillatory component with unknown coefficient $\alpha(\Omega, y_0)$. With a total of four unknown coefficients to be determined, the measurements of C_{x2} are included in the minimisation procedure, and the definition of the error becomes

$$\begin{aligned} error = &\left(C_{ya;model} - C_{ya;meaured}\right)^2 + \left(C_{yv;model} - C_{yv;meaured}\right)^2 \\ &+ \left(C_{x0;model} - C_{x0;meaured}\right)^2 + \left(C_{x2;model} - C_{x2;meaured}\right)^2 \end{aligned} \quad (35)$$

Attempts have been made to minimise the errors between the model results and the measured C_{ya}, C_{yv}, C_{x0} and C_{x2} with Eq.(35). However, at many data points, especially for a high amplitude $y_0 = 1.2$, it proved to be difficult to minimise the error such that it is smaller than 10^{-6}. More importantly, the large oscillating in-line forces C_{x2} at high frequencies and large amplitudes of cylinder oscillation can only be reproduced with the value of α in Eq.(32) being extremely

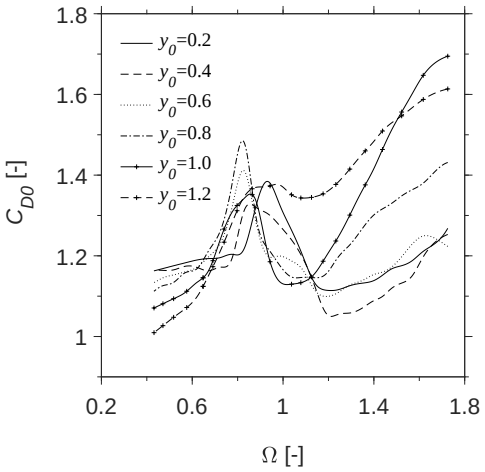

Figure 5: Frequency- and amplitude- dependent drag force coefficient obtained from the second drag force model.

large. This could be a result of the quadratic coupling relation between the lift and drag forces as derived from the stationary cylinder may to be no longer valid when the cylinder moves. However, it should be pointed out again that the influence of higher harmonics of the lift force is neglected here, and it is possible that to correctly model the oscillatory component of the in-line force, the higher harmonic components of the lift force need to be taken into account.

Since it is not possible to satisfy all four measurements with the third drag force model, an attempt was made to identify the lift force based on only three measurements, namely C_{ya}, C_{yv} and C_{x0}. With only three types of measurements to satisfy, one of the two parameters – $C_{D0}(\Omega, y_0)$ and $\alpha(\Omega, y_0)$ – in the third drag force model needs to be specified in advance. From the first and second drag force models, the resulted C_{VL0} and ϕ_{VL} seem to be insensitive to the value of $C_{D0}(\Omega, y_0)$. Therefore, this study assumes that the value of $C_{D0}(\Omega, y_0)$ is fixed and taken as 1.1856. Then, the values of C_{VL0}, ϕ_{VL} and $\alpha(\Omega, y_0)$ are obtained by minimising the error defined by Eq.(34) with tolerance 10^{-6}. The results reveal that, although not exact, the values of C_{VL0} and ϕ_{VL} have similar patterns to those obtained from the first and second drag models. The main differences are observed at high frequencies. Three examples of C_{VL0} and ϕ_{VL} obtained at $y_0 = 0.4$, $y_0 = 0.8$ and $y_0 = 1.2$ are presented in Fig.6 in comparison with results from the first drag model. The corresponding values of $\alpha(\Omega, y_0)$ are plotted in Fig.7. When a cylinder oscillates at a low frequency, it is expected that the value of α should be the same as that obtained from the fixed cylinder. However, it can be seen from Fig.7 that the values of α generally increase from negative values at low frequencies to positive at high frequencies. This is in contrast to the fact that for a fixed cylinder, the value of α is positive [19]. With the obtained values of C_{VL0}, ϕ_{VL} and α, C_{x2} was calculated, the values of which are again found to be similar to those calculated with the first and second drag force models and hence not presented here.

2.4. Discussion on the dynamic characteristics of the lift force

In the previous subsection, the lift forces that satisfy the experimental results have been identified based on three drag force models. The dynamic characteristics of the lift force obtained from

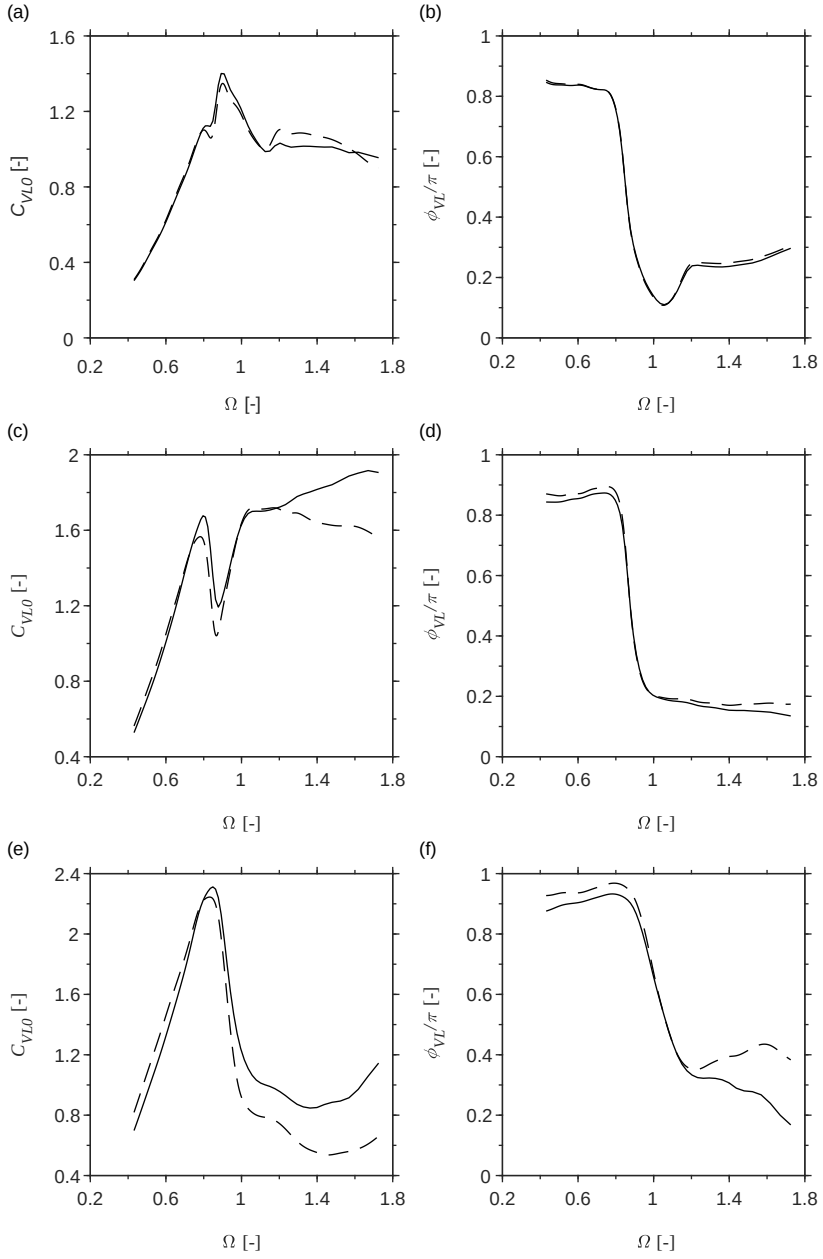

Figure 6: A comparison of the oscillatory lift force coefficients obtained from the first (dashed line) and third (solid line) drag force models at different amplitudes of cylinder oscillation (a,b) $y_0 = 0.4$, (c,d) $y_0 = 0.8$ and (e,f) $y_0 = 1.2$.

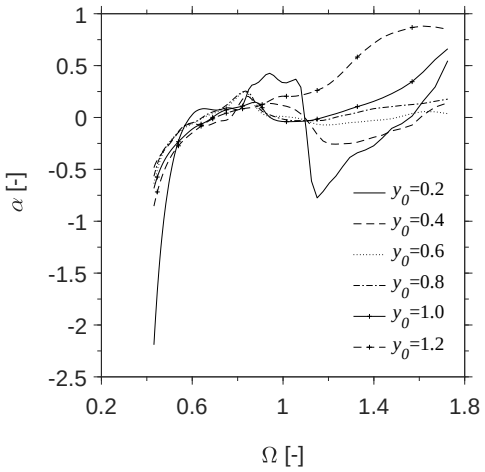

Figure 7: Frequency- and amplitude-dependent α obtained from the third drag force model.

the three models are almost the same. At a small amplitude of cylinder oscillation, the lift force reproduces the resonance phenomenon, which somehow reveals the similarity between the wake dynamics and an oscillator. However, at medium and large amplitudes, the dynamic characteristics of the lift force are such that the phase change still follows the resonance pattern, while the amplitude of the lift force does not. The contradiction to the resonance pattern at medium and large amplitudes of cylinder oscillation can explain why, in the work by Ogink and Metrikine [15], the wake oscillator model with frequency-dependent coupling only works well for small amplitudes of vibration.

One possible explanation for the contradiction could be the neglected added mass in the instantaneous flow direction (only the ideal added mass is accounted for in this direction). To fulfil the experimental results, the lift force is designed to compensate for the added mass component missed in the instantaneous flow direction, which could result in the misdistribution between the inertia and damping components of the lift force. Another possible explanation is the higher harmonic components. In the analysis conducted in this section, only the component at the frequency of cylinder oscillation is considered. It is possible that at medium and high amplitudes, the dynamics of the lift force are such that there are substantial energy transfers to other frequencies at the point of resonance due to some unaccounted for nonlinear mechanism. This can result in the reduction in the amplitude of lift force at the fundamental frequency, as observed.

Although taking into account the added mass effect due to the dynamics of the wake in the instantaneous flow direction may be crucial in the formulation of the hydrodynamic force model, the form in which the added mass should be incorporated into the model is still unclear and will not be investigated further. Therefore, in the next section the focus will still be placed on the improvement of the nonlinearity of the wake oscillator equation.

3. Improved wake oscillator model with nonlinear coupling

In the work by Ogink and Metrikine [15], the main goal was to develop a wake oscillator model that is able to reproduce both free and forced vibration experiments. Attempts have been made

to achieve this goal by making the linear coupling used in the classical wake oscillator models frequency-dependent. However, one of the main problems they encountered is that they were not able to find one set of frequency-dependent coefficients that would satisfy the forced vibration experiments at different amplitudes of cylinder oscillation. This is an indication of the improper nonlinearity used in the model. One of the possible improvements to the model is to use another nonlinear oscillator instead of the van der Pol equation. Utilising the van der Pol oscillator in the first place is barely an assumption, and any nonlinear oscillator that generates a limit cycle can potentially be used in the description of vortex formation. However, several studies have demonstrated that the van der Pol equation describes well the vortex shedding process [22, 23], which makes it unreasonable to replace that equation. Another possible approach is to introduce nonlinear coupling, which has not been studied before and therefore forms the focus of this paper.

Without knowing the exact type of nonlinear coupling that should be used, a reasonable start would be to represent the nonlinearities in the form of polynomials as multiplications of the displacement, velocity and acceleration of cylinder oscillation. If the nonlinearities of the coupling are polynomial in nature, then this representation should theoretically be able to model the system well for all frequencies and amplitudes of cylinder oscillation. If that is not the case, then according to the Weierstrass approximation theorem, the system can still be approximated to an arbitrary accuracy by polynomials within a given range of frequencies and amplitudes of cylinder oscillation. However, this is accompanied by the drawback of using high-order polynomials, which make the model too complicated and potentially unstable. Therefore, a combination of low-order polynomials is adopted here.

3.1. Description of the nonlinear coupling

The nonlinear couplings used in this section are given as

$$S = \sum_{n=0}^{3}\left[\frac{A_n}{D^{n+1}}|Y|^n\frac{d^2Y}{dt^2} + \omega_s\frac{B_n}{D^{n+1}}|Y|^n\frac{dY}{dt}\right], \quad \text{n is interger} \tag{36}$$

The above equation describes a combination of nonlinearities that are dependent on the displacement of cylinder motion up to a cubic term. Using the dimensionless parameters given in Eq.(16), the dimensionless form of Eq.(36) is obtained as

$$s = \sum_{n=0}^{3}\left[A_n|y|^n\ddot{y} + B_n|y|^n\dot{y}\right] \tag{37}$$

The nonlinear coupling terms inevitably result in a force on the wake oscillator that contains multiple frequency components. Here, it is assumed that the influence of the frequency components other than that of cylinder oscillation on the response of the oscillator is negligible. By substituting the cylinder motion $y = y_0\sin(\Omega\tau)$ into Eq.(37) and applying a Fourier series expansion, the force component acting on the wake oscillator at the frequency of cylinder oscillation can be obtained as

$$\begin{aligned} s_\Omega = &-(A_0 + \frac{8}{3\pi}A_1y_0 + \frac{3}{4}A_2y_0^2 + \frac{32}{15\pi}A_3y_0^3)y_0\Omega^2\sin(\Omega\tau) \\ &+(B_0 + \frac{4}{3\pi}B_1y_0 + \frac{1}{4}B_2y_0^2 + \frac{8}{15\pi}B_3y_0^3)y_0\Omega\cos(\Omega\tau) \end{aligned} \tag{38}$$

Comparing Eq.(38) with Eq.(23), the following expressions for A and B are obtained

$$A = A_0 + \frac{8}{3\pi}A_1 y_0 + \frac{3}{4}A_2 y_0^2 + \frac{32}{15\pi}A_3 y_0^3, \quad B = B_0 + \frac{4}{3\pi}B_1 y_0 + \frac{1}{4}B_2 y_0^2 + \frac{8}{15\pi}B_3 y_0^3 \tag{39}$$

Eq.(39) demonstrates that by considering only the excitation on the wake oscillator at the frequency of cylinder oscillation, the new nonlinear coupling terms can be expressed as acceleration and velocity couplings with amplitude-dependent coefficients A and B. The amplitude dependency is described by cubic polynomials given be Eq.(39). It has been pointed out by Ogink and Metrikine [15] that to comply with the measurements from the forced vibration experiment, the coupling coefficients A and B should also be frequency-dependent, which is not considered here. Still the model is tuned in the next subsection to investigate the extent to which it can reproduce the forced and free vibration experiments.

3.2. Tuning of the model to the forced vibration experiments

In this and the following subsections, the improved wake oscillator model with nonlinear coupling proposed in Section 3.1 is tuned to both forced and free vibration experiments. When doing this, one can start by tuning the model to the forced vibration experiments and then, with the same tuning parameters, conduct free vibration simulations and compare the results with experimental data, or vice versa. Here, the first approach is taken.

Since the objective of this part is to tune the model to the forced vibration experiments by Gopalkrishnan [20], it is reasonable to use $C_{D0} = 1.1856$, $C_{L0} = 0.3842$ and $\mathrm{St} = 0.1932$, as measured in the experiments. This leaves tuning parameters A_0, A_1, A_2, A_3, B_0, B_1, B_2, B_3 and ϵ to be determined. The large number of tuning parameters makes the model difficult to be tuned. Therefore, an alternative approach is taken here to determine the values of the tuning parameters.

As described in Section 3.1, if only the force component acting on the wake oscillator at the frequency of cylinder oscillation is considered, then the nonlinear coupling described by Eq.(37) formulates amplitude-dependent coefficients A and B. The amplitude dependency is given by Eq.(39). The amplitude-dependent A and B can be obtained by tuning the wake oscillator model Eqs.(22) and (23) to the forced vibration measurements at each amplitude. Then, the values of the nonlinear coupling coefficients A_0, A_1, A_2, A_3, B_0, B_1, B_2 and B_3 can be determined by finding the best fit of A and B against the amplitude of cylinder oscillation using Eq.(39).

To model the forced vibration, Eqs.(22) and (23) are solved numerically in the time domain, using a fifth-order Runge-Kutta method. The simulation runs for 150 periods of cylinder oscillation at a certain reduced velocity, and only the steady response of the last 50 periods is used for the analysis. With Eqs.(26) and (27), the coefficients C_{ya} and C_{yv} are calculated by averaging over the last 50 periods. The coefficients have been determined over the range of reduced velocities from $V_r = 3$ to $V_r = 12$ with a step size of $\mathrm{d}V_r = 0.1$.

When tuning Eqs.(22) and (23) to the forced vibration experiments, it is found that a smaller value of ϵ results in better agreement. However, a smaller ϵ also means a weak self-excitation in free vibration, as it decides the magnitude of negative added damping in the van der Pol kernel. Therefore, $\epsilon = 0.05$ is taken to achieve a suitable balance between self-excitation and the proper reproduction of the forced vibration experiments. Another problem encountered by the author is that Eqs.(22) and (23) cannot be exactly tuned to the forced vibration measurements at specified amplitudes of forced motion. This is actually expected, as Ogink and Metrikine [15] have already demonstrated that to reproduce the experimental results, the coupling coefficients, namely A and B, should be frequency-dependent. Despite of this drawback, a tuning result is considered to

be a good one if it covers the main trend of the measurements and quantitatively reproduces the negative C_{yv} over the range of reduced velocities $V_r = 5-8$, as this is the main range where VIV happens. With this criterion, a good set of tuning results is obtained and shown in Fig.8, in which dashed lines represent results of the model and solid lines are experimental measurements. The corresponding amplitude-dependent coefficients A and B are plotted in Fig.9 by squares.

To achieve the same tuning results by a wake oscillator with nonlinear coupling, which is described by Eqs.(22) and (37), tuning parameters A_0, A_1, A_2, A_3, B_0, B_1, B_2 and B_3 need to be carefully determined by finding an optimal fit of A and B with polynomials given by Eq.(39). Here, curve fittings are conducted using the least squares method, indicated by solid lines in Fig.9, and the corresponding nonlinear coupling coefficients are obtained as

$$\begin{aligned} &A_0 = 1.5, A_1 = 8.5, A_2 = -11.1, A_3 = 2.6; \\ &B_0 = 4.2, B_1 = 11.3, B_2 = -68.7, B3 = 50.5. \end{aligned} \tag{40}$$

With the values of the tuning parameters given by Eq.(40), Eqs.(22) and (37) are solved numerically with $y = y_0 \sin(\Omega\tau)$, and the coefficients C_{ya} and C_{yv} are determined by Eqs.(26) and (27) over the range of reduced velocities from 3 to 12 for amplitudes $y_0 = 0.2, 0.4$, until 1.2. The results are plotted in Fig.10 where the simulation results and experimental measurements are compared. From Fig.10, it can be seen that the simulation results of the wake oscillator model with nonlinear coupling are in fairly good agreement with the experimental measurements. Especially the excitation region, represented by negative C_{yv}, is well captured. According to the simulation results, the values of C_{yv} are negative at reduced velocities between approximately 5 and 8 at small amplitudes, which means a positive power input to the vibration of the cylinder under this regime. As the amplitude increases, the net power input into the vibration of the cylinder drops, and the values of C_{yv} become positive. For amplitudes larger than 0.8, the values of C_{yv} are positive over the whole range of reduced velocities. However, some disagreements from the comparison should also be noted. First, although the general decreasing trend of C_{ya} is captured for all amplitudes of cylinder oscillation, the negative values that are observed in experiments for a high reduced velocity, especially over the range of $V_r = 5-8$ where VIV normally occurs, have not been reproduced. It was found that although the fluid force C_{VY} modelled by the wake oscillator generates negative C_{ya}, it is the addition of the ideal inviscid inertial force that makes the total C_{ya} positive. There has been a continuing controversy about the applicability of the classical ideal inviscid added mass (with added mass coefficient $C_a = 1$) to the fluid force in the separated flows. Leonard and Roshko [24] believed that the ideal inviscid added mass of circular cylinder derived for the irrotational flow is also applicable generally in the problems of VIV based on a mathematical proof. However, Sarpkaya [2] argued that the proof given by Leonard and Roshko [24] only holds at the instant that a body is started from rest in a fluid otherwise at rest and the added mass coefficient C_a should not be always equal to unity in the unsteady flow (e.g., VIV). From our results shown in Fig.10, it seems that $C_a = 1$ leads to correct results at small reduced velocities, while at high reduced velocities a smaller value of C_a should be adopted to capture the negative C_{ya}. Note that the discrepancy of C_{ya} between the model and experimental results occurs at the reduced velocity $V_r \approx 6$ which corresponds to a change from 2S to 2P wake modes [21], which suggests that the applicability of $C_a = 1$ may not hold any more in the 2P wake pattern. Another main difference between the simulation results and experimental measurements shown in Fig.10 is that the model over-predicts the values of C_{yv} at low reduced velocities for all amplitudes. Especially for small amplitudes at $y_0 = 0.2$ and 0.4, the model fails to reproduce the negative C_{yv} around $V_r = 4$. Despite this discrepancy, the results of C_{yv} illustrated in Fig.10

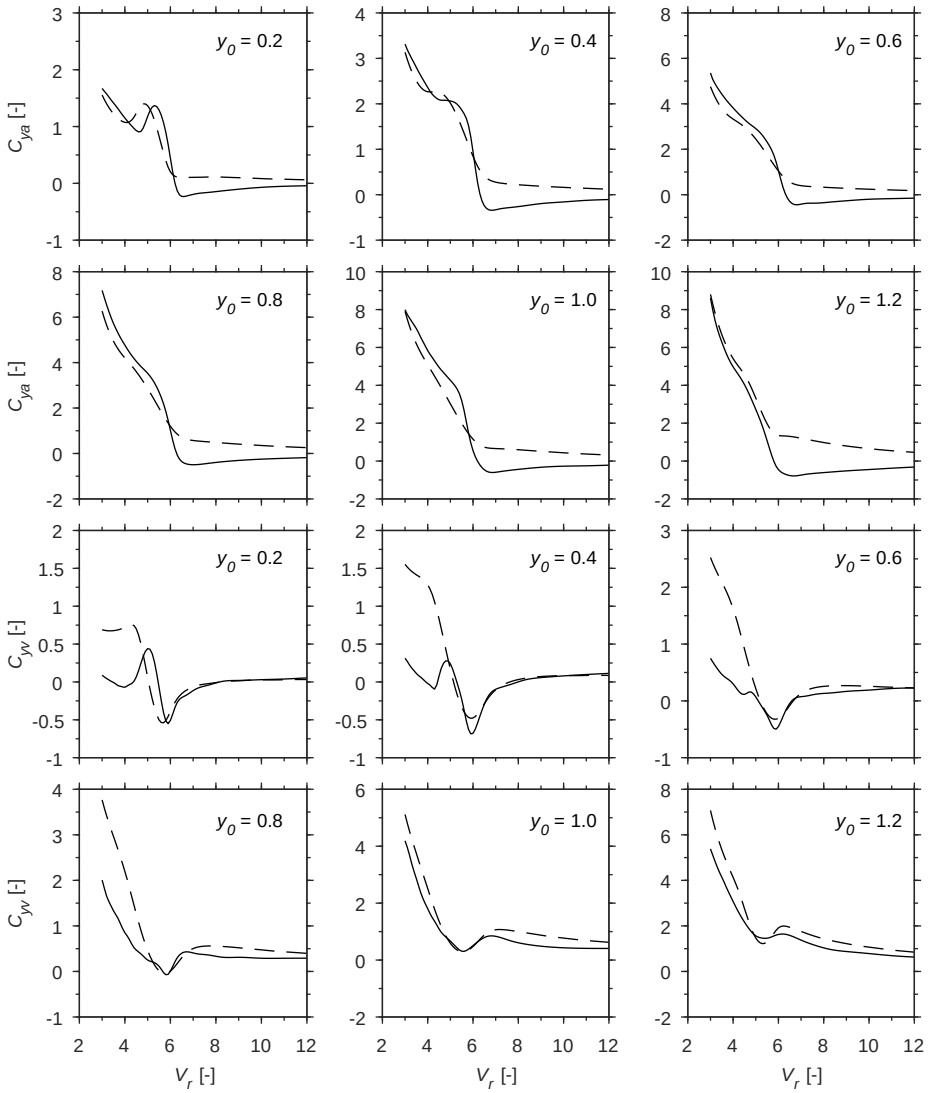

Figure 8: Tuning of the model to the forced vibration measurements at different amplitudes of cylinder oscillation. Solid lines represent measurements and dashed lines represent tuning results.

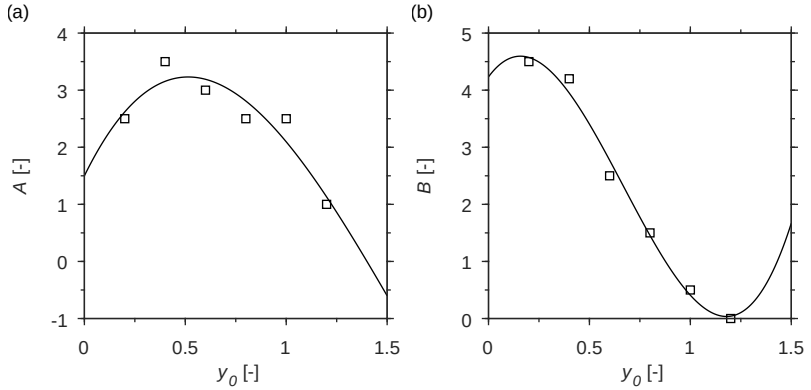

Figure 9: Determined values of (a) A and (b) B as a function of amplitude of cylinder oscillation (marked by squares), and curve fit (solid lines) found by least square method.

are considered to be acceptable because it is mainly the other excitation region at $V_r = 5-8$ that plays an important role in VIV.

3.3. Comparison with free vibration experiments

With the same tuning parameters given in Section 3.2, the wake oscillator model with nonlinear coupling is used to predict the vibration of an elastically supported rigid cylinder that is free to move only in the cross-flow direction. The coupled system of Eqs.(17), (18), (21) and (37) are solved numerically using a fifth-order Runge-Kutta method. The simulation runs for a time duration that corresponds to 150 cycles of vortex shedding (follows the Strouhal relation) at a certain reduced velocity V_n, and only the steady response of the last 50 cycles is used for analysis. The simulation results are presented with regard to the maximum amplitude A_y^* of dimensionless displacement and frequency ratio Ω/Ω_n. The A_y^* is determined by finding the maximum displacement recorded in the last 50 periods, and Ω is determined as the frequency corresponding to the highest peak in the Fourier spectrum of the analysed time series. This has been done for reduced velocities V_n ranging from 2 to 12 with a step $\mathrm{d}V_n = 0.1$. A series of experiments conducted by Khalak and Williamson [25] are used for the comparison. The reason for choosing these experiments is that they are in the range of Reynolds numbers similar to those in the experiments by Gopalkrishnan [20]. The simulation and experimental results are depicted in Fig.11. Different experiments are characterised by a different mass ratio m^* and mass-damping ratio $m^*\zeta$.

As seen in Fig.11, the main characteristics of the experiments are well captured. With similar mass-damping ratios $m^*\zeta$, the model predicts almost the same peak amplitudes for all three cases, and a wider lock-in range at a smaller mass ratio is also captured. This is consistent with the experimental finding that the peak amplitude is controlled principally by the product of $m^*\zeta$, whereas the range of lock-in is controlled primarily by m^* [25]. The maximum simulated amplitudes for all three cases are found at $V_n \approx 6$, with values around 0.8, while the results from the experiments reveal a slightly higher value at $V_n \approx 5$. This can be explained by the fact that the present parameters, namely C_{D0}, C_{L0} , St and the tuning parameters, are taken based on the forced vibration experiments that are conducted under a different condition.

From the comparison, a discrepancy can also be observed regarding the lock-in range and cylinder oscillation frequency for the small mass ratio case. The lock-in range is significantly

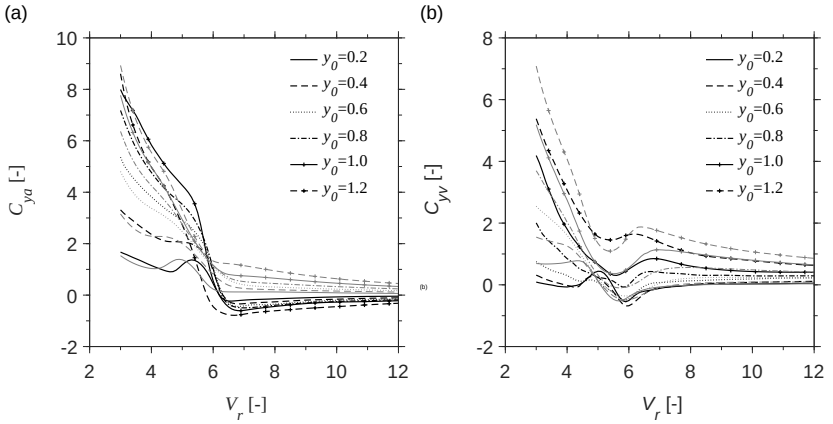

Figure 10: A comparison of the nonlinear coupling wake oscillator model (gray thin lines) and the forced vibration measurements (black thick lines) for the force coefficient (a) in phase with acceleration C_{ya} and (b) in phase with velocity C_{yv}.

underestimated by the model for the case $m^* = 2.4$. While the model predicts the vibration of the cylinder to reduce to negligible amplitudes for $V_n > 9$, the experiments indicate that the cylinder maintains a moderate oscillation until $V_n \approx 12$. As for the frequency of cylinder oscillation, the model predicts that the cylinder will vibrate at approximately the natural frequency of the system; this is consistent with the experimental results for $m^* = 10.3$ and $m^* = 20.6$. For the small mass ratio case, $m^* = 2.4$, the experiments demonstrate the deviation of the frequency of cylinder oscillation from the natural frequency. Within the lock-in range, the frequency of cylinder oscillation gradually increases with increasing reduced velocity and reaches a maximum value 1.5 times the natural frequency of the system. Although the rising trend of the frequency of cylinder oscillation is also observed in the simulation results, the model predicts much smaller values, with a maximum slightly higher than the natural frequency. The source of these discrepancies can be traced in the simulation results of the forced vibration experiments, as illustrated in Fig.10, where the model fails to capture the negative C_{ya}, analogous to negative added mass, over the range of oscillation frequencies where VIV takes place. The added mass introduced by the vortices has a significant influence on the response of the cylinder, especially for a small mass ratio system, since the natural frequency of the light cylinder when VIV occurs can be significantly different from that measured in still water. Without reproducing the negative added mass, it is expected that the model will predict a narrower lock-in range as well as a lower response frequency in free vibration simulations for small mass ratio systems.

Attempts have been made to capture the negative added mass without changing the added damping too much. This is difficult, as a frequency-dependent added mass is always accompanied by frequency-dependent added damping. Nevertheless, one possible way to achieve this goal is to introduce an additional restoring force. For detailed information and results, please refer to Appendix A. It has also been tried to improve the model by including velocity and acceleration dependent nonlinearities in addition to the Eq.(36). However, the model becomes difficult to be tuned and the performance of the model is marginally improved; see Appendix B.

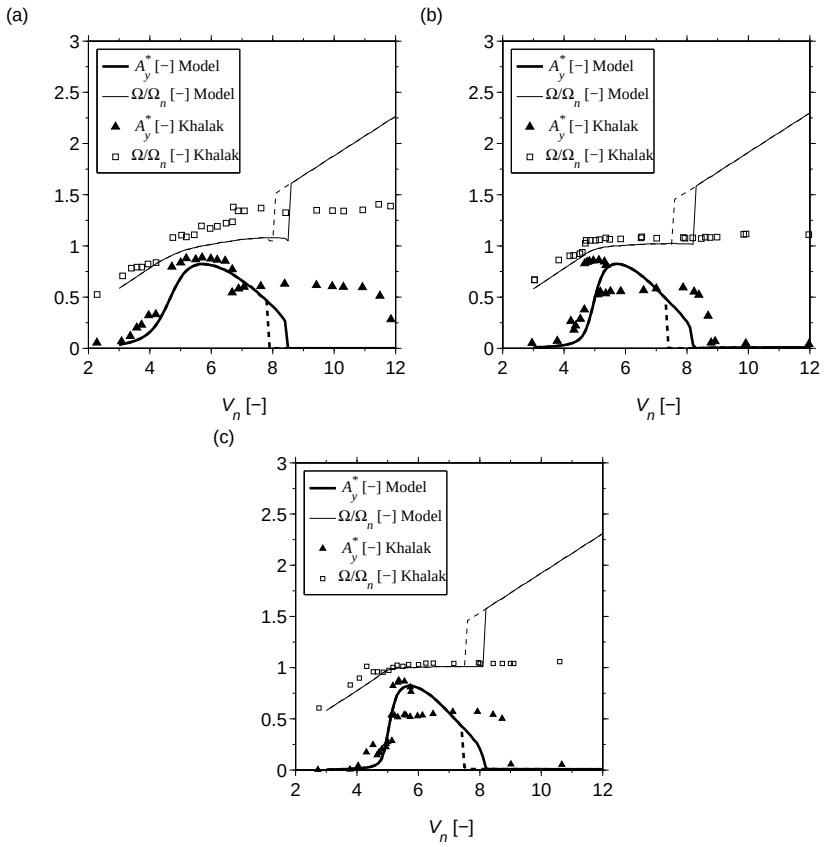

Figure 11: A comparison of the nonlinear coupling wake oscillator model and the free vibration measurements of Khalak and Williamson [25] for (a) $m^* = 2.4$,$m^*\zeta = 0.014$; (b)$m^* = 10.3$,$m^*\zeta = 0.017$; and (c) $m^* = 20.6$, $m^*\zeta = 0.019$. Solid lines represent quantities for increasing V_n, dashed lines for decreasing V_n.

4. Enhanced Model with frequency-dependent nonlinear coupling

As described in the previous section, a first attempt to improve the existing wake oscillator model by introducing nonlinear coupling terms is promising. However, one main drawback of the model is that it is not able to capture the negative added mass at high reduced velocities. In this section, the model is further enhanced by making the nonlinear coupling frequency-dependent.

4.1. Derivation of frequency-dependent nonlinear coupling

In the time domain, the frequency dependency can be achieved by means of convolution integrals, and the nonlinear terms follow the same form as those in Eq.(37). To make the model as simple as possible, this study starts with the coupling

$$s = \int_0^\tau h_0(\tilde{\tau})\dot{y}(\tau-\tilde{\tau})d\tilde{\tau} + \int_0^\tau h_1(\tilde{\tau})|y(\tau-\tilde{\tau})|\dot{y}(\tau-\tilde{\tau})d\tilde{\tau} + \int_0^\tau h_2(\tilde{\tau})y(\tau-\tilde{\tau})^2\dot{y}(\tau-\tilde{\tau})d\tilde{\tau} \quad (41)$$

which contains less nonlinear terms than Eq.(37). The reason for using less nonlinear terms is that the coupling given by Eq.(41) is already sufficient to generate a fairly suitable reproduction of the forced vibration measurements, as will be shown later.

Excitation on the wake oscillator, described by Eq.(41), contains multiple harmonic components due to nonlinearity. To have the formulas written in a clear format, the equations are formulated in a complex-valued form in the following part. Substituting the cylinder motion $y = -\mathrm{i}\frac{y_0}{2}(e^{\mathrm{i}\Omega\tau} - e^{-\mathrm{i}\Omega\tau})$ into Eq.(41), and assuming that the components at a frequency higher than 3Ω have a minor influence on the results, Eq.(41) can be approximated, using Fourier expansion, as

$$s \approx K_1 e^{\mathrm{i}\Omega\tau} + \bar{K}_1 e^{-\mathrm{i}\Omega\tau} - (K_3 e^{\mathrm{i}3\Omega\tau} + \bar{K}_3 e^{-\mathrm{i}3\Omega\tau}) \quad (42)$$

where

$$\begin{aligned} K_1 &= \frac{1}{2}y_0\Omega H_0(\Omega) + \frac{2}{3\pi}y_0^2\Omega H_1(\Omega) + \frac{1}{8}y_0^3\Omega H_2(\Omega) \\ K_3 &= \frac{1}{3\pi}y_0^2\Omega H_1(3\Omega) + \frac{1}{8}y_0^3\Omega H_2(3\Omega) \end{aligned} \quad (43)$$

and when steady state is reached, i.e. $\tau \to \infty$,

$$H_0(\Omega) = \int_0^\infty h_0(\tilde{\tau})e^{-i\Omega\tilde{\tau}}d\tilde{\tau} \quad (44)$$

$$H_1(\Omega) = \int_0^\infty h_1(\tilde{\tau})e^{-i\Omega\tilde{\tau}}d\tilde{\tau} \quad (45)$$

$$H_2(\Omega) = \int_0^\infty h_2(\tilde{\tau})e^{-i\Omega\tilde{\tau}}d\tilde{\tau} \quad (46)$$

The overbar in the equations above and in the remainder of this chapter designates the complex conjugation.

Eqs.(44-46) indicate that the time domain kernels $h_0(t)$, $h_1(t)$ and $h_2(t)$ are the inverse Laplace transforms of $H_0(\Omega)$, $H_1(\Omega)$ and $H_2(\Omega)$ respectively provided that the Laplace variable s is given by $\mathrm{s} = \mathrm{i}\Omega$. To find the kernels of the convolution integrals, $H_0(\Omega)$, $H_1(\Omega)$ and $H_2(\Omega)$ must first

be determined. This can be done by tuning the wake oscillator model described by Eqs.(22) and (42) to the forced vibration experiments at each frequency.

The steady state solution of Eqs.(22) and (42) can be sought for in the form of $q = q_1 e^{\mathrm{i}\Omega\tau} + \bar{q_1} e^{-\mathrm{i}\Omega\tau} + q_3 e^{\mathrm{i}3\Omega\tau} + \bar{q_3} e^{-\mathrm{i}3\Omega\tau}$. Substituting the latter expression into Eqs.(22) and (42), a collection of multipliers of $e^{\mathrm{i}\Omega\tau}$ and $e^{\mathrm{i}3\Omega\tau}$ yields two equations:

$$\begin{aligned} -\mathrm{i}\epsilon q_1^2 \bar{q_3}\Omega + \bar{q_1} + \mathrm{i}\epsilon \bar{q_1}\Omega - 2\mathrm{i}\epsilon q_3 \bar{q_3} \bar{q_1}\Omega - \mathrm{i}\epsilon q_1 {\bar{q_1}}^2 - \bar{q_1}\Omega^2 - K_1 = 0 \\ -\mathrm{i}\epsilon {\bar{q_1}}^3\Omega + 3\mathrm{i}\epsilon \bar{q_3}\Omega - 9\bar{q_3}\Omega^2 - 3\mathrm{i}\epsilon q_3 {\bar{q_3}}^2\Omega + \bar{q_3} - 6\mathrm{i}\epsilon q_1 \bar{q_1} \bar{q_3}\Omega + K_3 = 0 \end{aligned} \tag{47}$$

The hydrodynamic coefficients C_{ya} and C_{yv} are measured at the frequency of cylinder oscillation, and Eqs.(26) and (27) can be rewritten in the complex form as

$$\begin{aligned} -C_{yv} + \mathrm{i}C_{ya} =& \frac{2}{T}\int_{\tau_0}^{\tau_0+T} C_y \exp(\mathrm{i}\Omega\tau)\, d\tau \\ =& \frac{2}{T}\int_{\tau_0}^{\tau_0+T} C_{VY} \exp(\mathrm{i}\Omega\tau)\, d\tau + \mathrm{i}C_a \pi^3 \mathrm{St}^2 \Omega^2 y_0 \end{aligned} \tag{48}$$

Substituting $q = q_1 e^{\mathrm{i}\Omega\tau} + \bar{q_1} e^{-\mathrm{i}\Omega\tau} + q_3 e^{\mathrm{i}3\Omega\tau} + \bar{q_3} e^{-\mathrm{i}3\Omega\tau}$ and $y = -\mathrm{i}\frac{y_0}{2}(e^{\mathrm{i}\Omega\tau} - e^{-\mathrm{i}\Omega\tau})$ into Eq.(48) results in

$$\begin{aligned} -C_{yv} + \mathrm{i}C_{ya} \approx & \sqrt{1 + 4\pi^2 S t^2 \Omega^2 y_0^2}\left(-\frac{1}{2}q_1 C_{L0} - \frac{1}{4}\bar{q_1} C_{L0} + \frac{3}{2}\pi S t y_0 C_{D0}\Omega\right) - \frac{1}{2}q_1 C_{L0} \\ & + \frac{1}{4}\bar{q_1} C_{L0} + \frac{1}{2}\pi S t y_0 C_{D0}\Omega + 2iC_a \pi^3 S t^2 y_0 \Omega^2 \\ & + \frac{1}{4}q_3 C_{L0}\left(\sqrt{1 + 4\pi^2 S t^2 \Omega^2 y_0^2} - 1\right) \end{aligned} \tag{49}$$

The approximation in Eq. (49) is obtained using

$$\sqrt{1 + 4\pi^2 S t^2 y_0^2 \Omega^2 \cos(\Omega\tau)^2} \approx \frac{1}{2}\sqrt{1 + 4\pi^2 S t^2 y_0^2 \Omega^2}\,(1 + \cos(2\Omega\tau)) + \frac{1}{2}(1 - \cos(2\Omega\tau)) \tag{50}$$

At a specific frequency Ω, if the values of $H_0(\Omega)$, $H_1(\Omega)$,$H_2(\Omega)$, $H_1(3\Omega)$ and $H_2(3\Omega)$ are already known, C_{ya} and C_{yv} at a certain amplitude y_0 can be calculated by solving algebraic equations Eqs.(47) and (49). Likewise, with measurements of C_{ya} and C_{yv} known, the values of $H_0(\Omega)$, $H_1(\Omega)$,$H_2(\Omega)$, $H_1(3\Omega)$ and $H_2(3\Omega)$ can be determined by solving the system of equations composed of Eqs.(47) and (49) at five amplitudes y_0.

Using the method described above, attempts were made to tune the model to the forced vibration experiments at different combinations of five amplitudes y_0. However, no solution was found through Eqs.(47) and (49). A possible reason, in the authors' opinion, is that the component of Eq.(41) at frequency 3Ω has a negligible influence on the results. Thus, instead of being tuned to five amplitudes at each frequency, the model is tuned to three amplitudes by solving Eqs.(47) and (49), with $K_3 = 0$. Some of the tuning results using different combinations of amplitudes are presented in Fig.12.

If the nonlinear couplings used in Eq.(41) are correct, then the choice of the three amplitudes to which the model is tuned should theoretically not affect the results in a significant way. However, from Fig.12, it can be seen that this is not the case here. The tuning results are highly sensitive to the choice of amplitudes, which is a strong indication that the coupling terms used here do

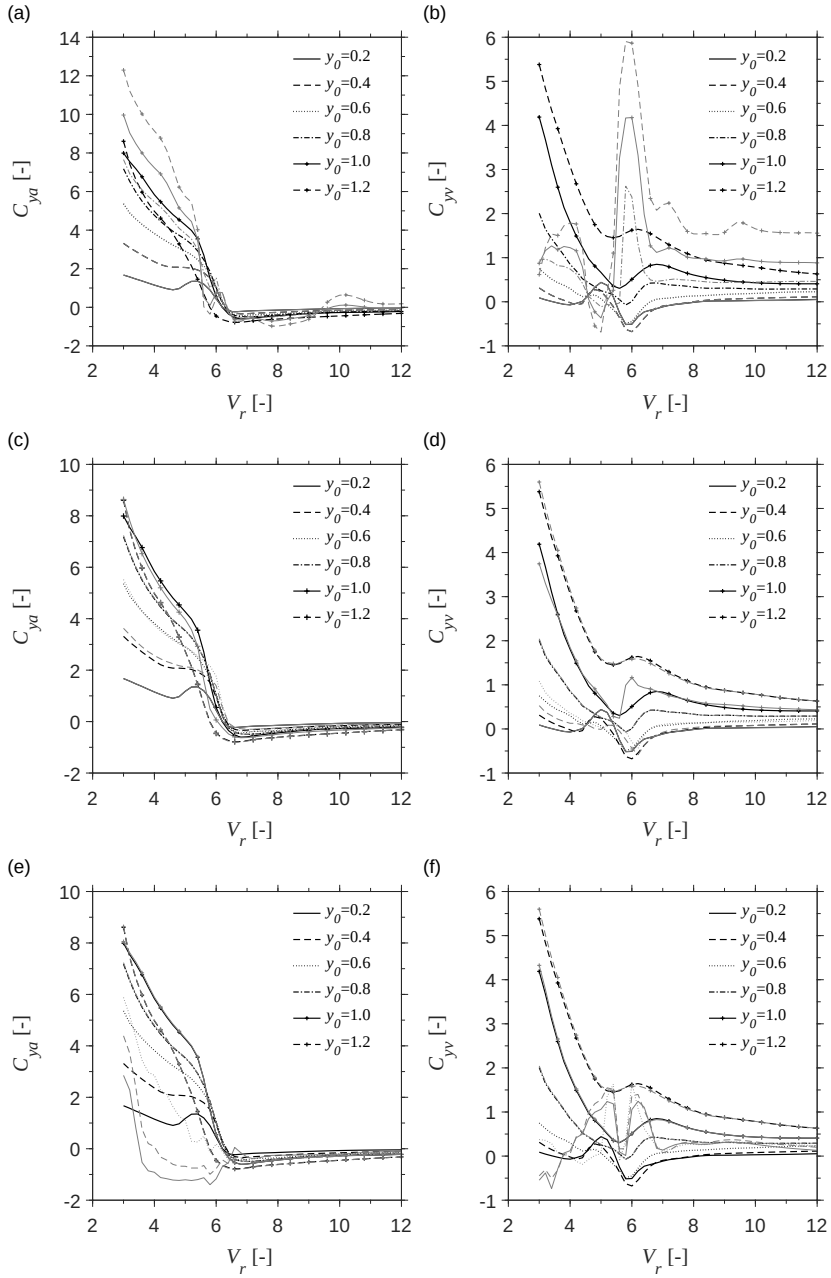

Figure 12: Tuning of the model with nonlinear coupling to the forced vibration measurements at amplitudes (a,b) $y_0 = 0.2, 0.4, 0.6$; (c,d) $y_0 = 0.2, 0.8, 1.2$; and (e,f) $y_0 = 0.8, 1.0, 1.2$. Black thick lines represent measurements and gray thin lines represent tuning results.

not contain the correct nonlinearities. Despite this conclusion, it was found that with current model, it is possible to obtain an acceptable reproduction of experiments by tuning the model to $y0 = 0.2, 0.8, 1.2$; see plot (b) in Fig.12. The corresponding $H_0(\Omega)$, $H_1(\Omega)$ and $H_2(\Omega)$ are presented in Fig.13.

4.2. Determination of the convolution kernels

In the previous subsection, the values of $H_0(\Omega)$, $H_1(\Omega)$ and $H_2(\Omega)$ have been determined within a finite frequency range according to the forced vibration experiments. Also, it has been demonstrated that the kernels $h_0(t)$, $h_1(t)$ and $h_2(t)$ are given by the inverse Laplace transforms of $H_0(\Omega)$, $H_1(\Omega)$ and $H_2(\Omega)$. However, before performing an inverse Laplace transform, the values of $H_0(\Omega)$, $H_1(\Omega)$ and $H_2(\Omega)$ within a finite range of frequencies need to be extended to the entire frequency domain. This process of extension is not arbitrary. To obtain a kernel in the time domain, the frequency domain values need to be extended following the Kramers-Kronig relations [26] so that the principle of causality is satisfied. For a complex function $\chi(\Omega) = \chi_1(\Omega) + i\chi_2(\Omega)$, the Kramers-Kronig relations are given by

$$\begin{aligned} \chi_1(\Omega) &= \frac{2}{\pi}\mathcal{P}\int_0^\infty \frac{\Omega'\chi_2(\Omega')}{\Omega'^2 - \Omega^2}d\Omega' \\ \chi_2(\Omega) &= -\frac{2\Omega}{\pi}\mathcal{P}\int_0^\infty \frac{\chi_1(\Omega')}{\Omega'^2 - \Omega^2}d\Omega' \end{aligned} \tag{51}$$

where $\mathcal{P}$ denotes the Cauchy principle value. In this study, both real and imaginary parts are available only in a limited range of frequencies, which makes it impossible to extend them to the whole frequency domain by directly applying Eq.(51). Therefore, in this paper, the spectrum of $H_0(\Omega)$, $H_1(\Omega)$ and $H_2(\Omega)$ is extended with complex curve fitting. The basic idea of this method is to approximate the frequency domain responses with basic functions that already meet Kromers-Kronig relations. The most widely used general fitting methodology was proposed by Gustavsen and Semlyen [27], and it is used to fit the measured or calculated frequency domain responses with rational function approximations. The same method will be used in this paper.

According to Gustavsen and Semlyen [27], a complex function $H(\Omega)$ can be approximated as

$$H(\Omega) = \sum_{n=1}^{N}\left(\frac{c_n}{\mathrm{i}\Omega - a_n} + \frac{\bar{c_n}}{\mathrm{i}\Omega - \bar{a_n}}\right) + d + \mathrm{i}\Omega h \tag{52}$$

where the residual c_n and poles a_n are either real or complex quantities, while d and h are real. The inverse Laplace transform of Eq.(52) results in the kernel $h(\tau)$ as

$$h(\tau) = \sum_{n=1}^{N}[2\exp(a_n^{\mathrm{re}})(c_n^{\mathrm{re}}\cos(a_n^{\mathrm{im}}\tau) - c_n^{\mathrm{im}}\sin(a_n^{\mathrm{im}}\tau))] + d\delta(\tau) + h\frac{d}{d\tau}\delta(\tau) \tag{53}$$

in which δ denotes the Dirac delta function, and the superscripts 're' and 'im' denote the real and imaginary parts of c and a. From Eq.(53) it can be noted that the poles a should have negative real parts to ensure that $\lim_{\tau\to\infty} h(\tau) = 0$.

Another advantage of using Eq.(52) for the approximation is that once the kernels are identified, the convolutions can be replaced by a set of ordinary differential equations. Solving these equations in the time domain is significantly more efficient than calculating integrals associated with the convolutions.

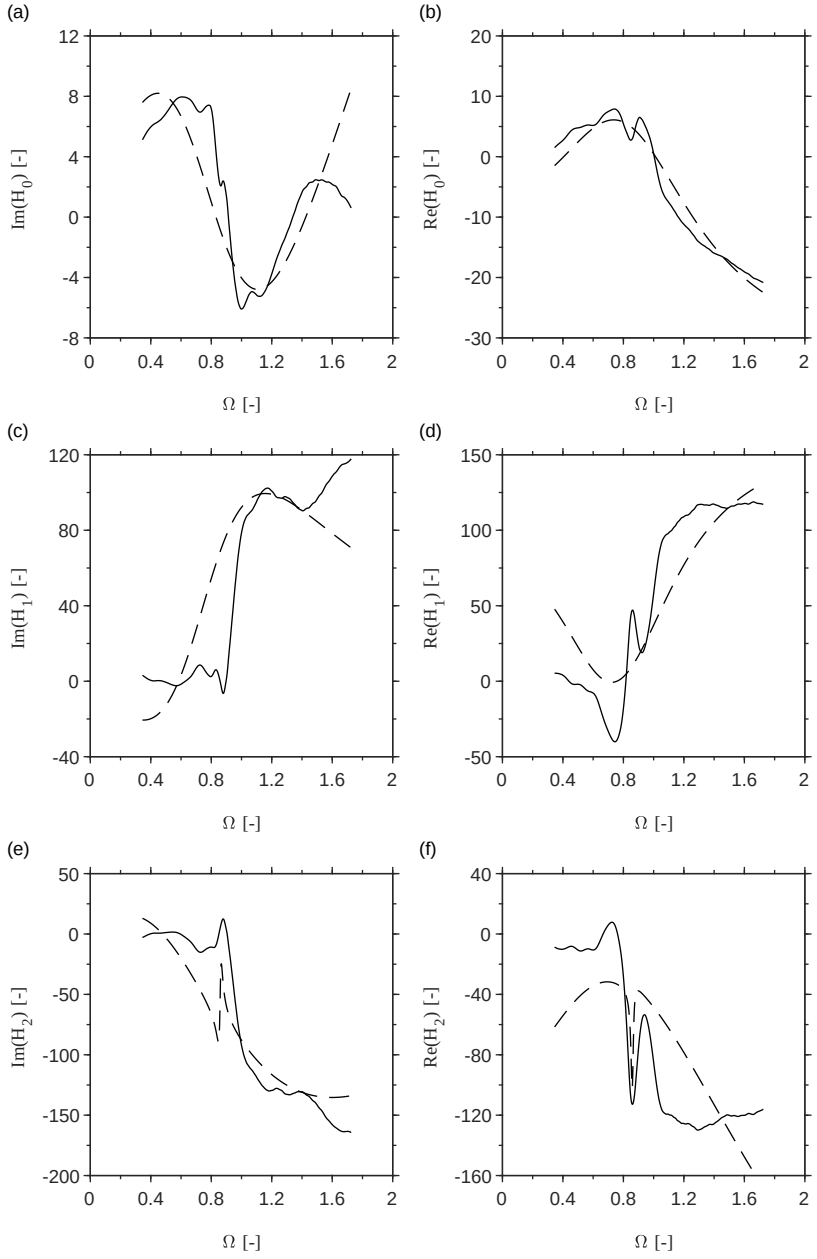

Figure 13: Frequency-dependent (a,b) $H_0(\Omega)$, (c,d) $H_1(\Omega)$ and (e,f) $H_2(\Omega)$ determined from the forced vibration measurements, represented by solid lines, as well as curve fitting results, represented by dashed lines.

Using this method, attempts were made to fit the complex curves of $H_0(\Omega)$, $H_1(\Omega)$ and $H_2(\Omega)$, as illustrated in Fig.13, with a well-developed tool that is publicly available online. However, obtaining good fits for all three curves with this method was found to be impossible. For $H_0(\Omega)$, positive a_n^{re} are encountered for fitting results with $N > 2$. For $H_1(\Omega)$ and $H_2(\Omega)$, this study did not find any fit, as regardless of the number of poles used, poles with positive real parts always exist. By imposing constraints of $a_n^{\mathrm{re}} < 0$ on the process of approximation, it is possible to obtain some fitting results for $H_1(\Omega)$ and $H_2(\Omega)$. However, these fitting results are poor. Fig.13 presents the fitting results of the three curves with $N = 2$. Approximations have also been conducted with $N > 2$, but it was found that increasing the number of poles does not improve the fitting results.

The results of this section can be summarized as follows. The introduction of nonlinear coupling enables us to identify one set of frequency dependent functions that is valid at all amplitudes of forced vibration. This is a major improvements with respect to the work by Ogink and Metrikine [15] where at every amplitude of forced vibration a different set of frequency dependencies needs to be applied. Despite of this improvement, it has been shown impossible to extend these functional dependencies from the measured frequency interval to the infinite frequency domain, in a manner that conforms to the Kramers-Kronig relations and energy conservation, using the complex curve fitting method. The possible underlying reasons will be discussed in next section.

5. Conclusions

In this paper, the wake oscillator model proposed by Ogink and Metrikine [15] has been reviewed and improved to have a better prediction of both free and forced vibration experiments.

A review of the wake oscillator model proposed by Ogink and Metrikine [15] has emphasised the fact that the reproduction of the forced vibration measurements requires the appropriate modelling of both lift (a force that is perpendicular to the relative flow velocity) and drag (a force that is parallel to the relative flow velocity) forces. A deficient drag force model may make it difficult, if not impossible, to formulate the lift force, as the lift needs to compensate for the errors introduced by the drag force. Three main discussable assumptions regarding the drag force model in Ref.[15] have been identified, namely making a quasi-steady assumption, ignoring the oscillatory components and neglecting the inertia force in the direction of the drag force. With regard to the first two assumptions, the characteristics of the dynamics of the oscillatory lift force – at the frequency of cylinder oscillation – that satisfy the forced vibration experimental measurements are analysed based on three different drag force models. The first model is the one proposed by Ogink and Metrikine [15]; it assumes that the instantaneous drag force coefficient is constant and keeps the mean steady value measured on the fixed cylinder. In the second model, the instantaneous drag force coefficient is still assumed to be constant; however, its value varies as the frequency or amplitude of cylinder motion changes. In the third model, in addition to the constant drag force, an oscillatory part coupled with the lift force is introduced, and the coupling relation keeps the same form as that identified from a fixed cylinder. It has been demonstrated that the oscillatory lift forces determined from the three drag force models are similar, which suggests that the first drag force model is at least not more deficient than the other two. The characteristic of the dynamics of the identified lift force exhibits an obvious resonance pattern at small amplitudes of cylinder oscillation, while it is contradictory to the resonance pattern at large amplitudes. The contradiction may be a result of neglecting the inertia force in the direction of the drag force or simply due to a wrongly chosen nonlinearity.

Since the drag force models do not have a significant influence on the reproduction of the forced vibration experiments, the first drag force model is applied, and the possibility of improving the reproduction of the forced vibration experiments by introducing extra nonlinearity in the wake oscillator equation is investigated. The nonlinearity has been introduced through the coupling between the wake oscillator equation and the cylinder motion. As a preliminary test, a set of nonlinear coupling terms in the form of multiplications of displacement, velocity and acceleration of the cylinder have been introduced. The model with constant coupling coefficients has been shown to be able to quantitatively reproduce the added damping measured in the forced vibration experiments over most of the range of frequencies and amplitudes that are of interest; however, that model fails to capture the negative added mass at high reduced velocities. It was found that although the wake oscillator model generates negative added mass, the addition of the ideal inviscid added mass makes the total positive, which suggests that the applicability of added mass coefficient $C_a = 1$ may not hold any more at high reduced velocities where the wake pattern is in 2P mode. The importance of the negative added mass has been reflected in the simulation of free vibration experiments where the model was shown to underestimate the lock-in range as well as the frequency of the cylinder oscillation for the system with a small mass ratio. A remedy has been proposed to overcome this discrepancy by introducing additional restoring force.

In order to obtain a perfect reproduction of the forced and free vibration tests, it has been attempted to make the nonlinear coupling coefficient frequency-dependent; this is achieved in the time domain by means of convolution integrals. A single set of frequency-dependent complex-valued functions, which are the Laplace transforms of corresponding convolution kernels, that reproduces the forced vibration experiments fairly well at different amplitudes of vibration has been identified over a limited frequency range. Finding such a set of frequency-dependent complex-valued functions has been shown to be impossible for linear coupling [15]. Despite of this major improvement, an attempt to extend the functional dependencies to the infinite frequency domain using a complex curve fitting method such that the principle of causality and energy conservation are satisfied failed also in the case of the nonlinear frequency-dependent coupling. In authors' opinion, there are two possible explanations to this. One explanation is that the nonlinearities, which are essentially in the form of polynomials, that have been used in this paper are not adequately accurate to reproduce the results of both the forced and free vibration tests. It is possible that if the intrinsic nonlinearities in the process of VIV are not in the form of polynomials, then no matter how good a reproduction of the experimental forced vibration results is achieved in the frequency domain we may always fail to transform it into the time domain following the principle of causality and energy conservation. If this is true, then the focus of the future research should be placed on identifying the intrinsic nonlinearities of VIV, which is apparently challenging. Another possible explanation is that the complex curve fitting method based on rational basic functions that has been used in this paper, despite of its wide applications, is not applicable to this specific case. It is thus recommended to try other methods or use different basic functions to identify the convolution kernels in the future study.

Although the attempt to develop a wake oscillator model that can perfectly reproduce the experimental forced and free vibration results has failed, the model has been significantly improved in this work by introducing nonlinear couplings with constant coefficients. A natural next step of this work would be implementing this improved model to simulate VIV of flexible cylinders. For flexible cylinders, the model would have to be further modified to take in-line motion into account, such that coupled cross-flow and in-line VIV can be simulated.

6. Acknowledgements

The first author would like to thank the China Scholarship Council (CSC) (No. 201206450001) for the financial support to this work.

Appendix A. Capturing the negative added mass by introducing an extra restoring force

The added mass plays an important role in VIV, and the negative added mass observed in the forced vibration experiments is the main reason for the wider lock-in range and higher lock-in frequency for low mass ratio systems compared to high mass ratio systems in free vibration tests. It has been shown in Section 3 that the added mass is well reproduced at a high frequency of cylinder oscillation, while it does not seem to be possible to capture the negative added mass at low frequencies of cylinder oscillation. It was found that at a low frequency of cylinder oscillation, even though the portion of the added mass contributed by the wake oscillator is negative, the addition of the potential added mass makes the total positive. It seems the assumption of the potential added mass coefficient C_a's constant value of 1 is only applicable at a high frequency of cylinder oscillation, while a smaller or even negative value should be taken when the cylinder oscillates at a low frequency. To achieve this goal, the cross-flow hydrodynamic force F_{AY} in Eq.(2) is reformulated as

$$F_{AY} = -m_{a0}\frac{d^2Y}{dt^2} - m_{a1}\omega_s^2 Y \tag{A.1}$$

in which the first term is still the inertia force and added mass $m_{a0} = C_{a0}\pi\rho LD^2/4$, while the second term is a restoring force and $m_{a1} = C_{a1}\pi\rho LD^2/4$. Physically, adding a restoring force in the formulation of a hydrodynamic force seems to be irrational, since for an immersed cylinder, the fluid forces acting on it should not be dependent on the displacement. However, this addition does improve the model's performance.

With the new definition of cross-flow inertia force F_{AY}, as given by Eq.(A.1), the equivalent potential added mass coefficient of the system becomes

$$C_a = \frac{F_{AY}}{\frac{1}{4}\rho\pi LD^2\frac{d^2Y}{dt^2}} = C_{a0} - C_{a1}\omega_s^2\frac{Y}{\frac{d^2Y}{dt^2}} \tag{A.2}$$

The dimensionless form of above equation is given as

$$C_a = C_{a0} + C_{a1}\frac{y}{\ddot{y}} \tag{A.3}$$

By substituting $y = y_0\sin(\Omega\tau)$ into Eq. (A.3), one obtains

$$C_a = C_{a0} - \frac{C_{a1}}{\Omega^2} \tag{A.4}$$

Eq.(A.4) demonstrates that the addition of the restoring force makes the added mass coefficient C_a frequency-dependent, and its value decreases with a decreasing frequency of cylinder oscillation. With $\Omega = 1/\mathrm{St}/V_r$, Eq.(A.4) becomes

$$C_a = C_{a0} - C_{a1}\mathrm{St}^2V_r^2 \tag{A.5}$$

In still water, when the flow velocity V equals 0, the reduced velocity $V_r = 2\pi V/(\omega D) = 0$, and Eq.(A.5) should conform to the potential theory; therefore, the value for C_{a0} should be 1.

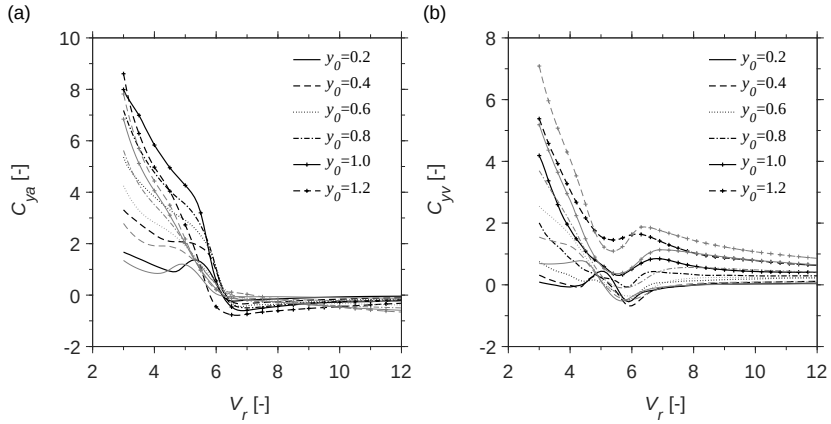

Figure A.14: A comparison of the nonlinear coupling wake oscillator model with the additional restoring force (gray thin lines) and the forced vibration measurements (black thick lines) for the force coefficient (a) in phase with acceleration C_{ya} and (b) in phase with velocity C_{yv}.

Regarding the value of C_{a1}, here $C_{a1} = 0.4$ is used to capture the negative values of C_{ya} at high reduced velocities. The forced vibration simulation results of C_{ya} with $C_{a0} = 1$ and $C_{a1} = 0.4$ are plotted in Fig.A.14 using the same tuning parameters as those given in Eq.(40). It can be seen that with this new term, the model captures the feature of negative values of C_{ya} at $V_c > 6$. According to the measurements, the values of C_{ya} decrease rapidly around $V_c = 6$ with increasing reduced velocity, reaching minimum negative values around $V_c = 7$ and then increasing gradually again, converging to a value slightly smaller than zero. However, the results from the model indicate no minimum value around $V_c = 7$, and the values keep decreasing, reaching values smaller than those observed in the measurements.

With the new added term in the inertia force, the non-dimensional form of the cylinder's equation of motion in Eq.(17) now becomes

$$\ddot{y} + 2\zeta\Omega_n\dot{y} + \Omega_n^2 y = \frac{1}{\pi(m^* + C_{a0})}\frac{1}{2\pi^3 \mathrm{St}^2}C_{VY} - C_{a1}\frac{y}{(m^* + C_{a0})} \tag{A.6}$$

Solving Eq.(A.6), (18) and (37), the free vibration with $m^* = 2.4, 10.3$ and 20.6 is simulated, and results are shown in Fig.A.15. Form Fig.A.15 it can be seen that the free vibration of the system with a small mass ratio is properly modeled with respect to the value of frequency and range of lock-in.

Appendix B. Velocity and acceleration dependent nonlinear couplings

In this section, the velocity and acceleration dependent nonlinear couplings, in addition to Eq.(37), are considered in the following equation

$$s = \sum_{n=0}^{3}\left[A_n|y|^n\ddot{y} + B_n|y|^n\dot{y}\right] + \sum_{n=1}^{2}\left[\tilde{A}_n|\dot{y}|^n\ddot{y} + \tilde{B}_n|\dot{y}|^n\dot{y}\right] + \hat{A}|\ddot{y}|\ddot{y} + \hat{B}|\ddot{y}|\dot{y} \tag{B.1}$$

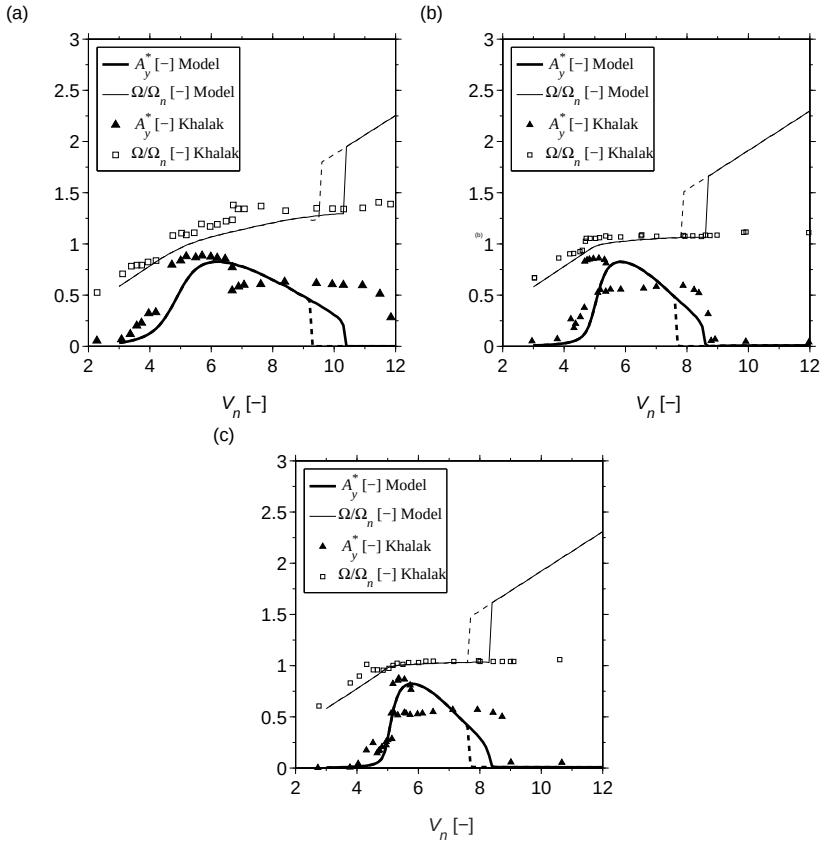

Figure A.15: A comparison of the nonlinear coupling wake oscillator model with the additional restoring force and the free vibration measurements of Khalak and Williamson [25] for: (a) $m^* = 2.4, m^*\zeta = 0.014$; (b)$m^* = 10.3, m^*\zeta = 0.017$; (c) $m^* = 20.6$, $m^*\zeta = 0.019$. Solid lines represent quantities for increasing V_n, dashed lines for decreasing V_n.

In the above equation, the velocity and acceleration dependent coupling terms have been chose to avoid high order polynomials. With 14 coefficients in Eq.(B.1), the model is difficult to be tuned. Therefore, a similar approach as that described in Section 3 is taken here. By substituting the cylinder motion $y = y_0 \sin(\Omega\tau)$ into above equation and applying a Fourier series expansion, we obtain the following expressions, considering only the components at the frequency of cylinder oscillation, for A and B

$$\begin{aligned} A &= A_0 + \frac{8}{3\pi}A_1 y_0 + \frac{3}{4}A_2 y_0^2 + \frac{32}{15\pi}A_3 y_0^3 + \frac{4}{3\pi}\tilde{A}_1\Omega y_0 + \frac{1}{4}\tilde{A}_2\Omega^2 y_0^2 + \frac{8}{3\pi}\hat{A}\Omega^2 y_0, \\ B &= B_0 + \frac{4}{3\pi}B_1 y_0 + \frac{1}{4}B_2 y_0^2 + \frac{8}{15\pi}B_3 y_0^3 + \frac{8}{3\pi}\tilde{B}_1\Omega y_0 + \frac{3}{4}\tilde{B}_2\Omega^2 y_0^2 + \frac{4}{3\pi}\hat{B}\Omega^2 y_0. \end{aligned} \tag{B.2}$$

Applying the minimization procedure described by Ogink and Metrikine [15], the amplitude and frequency dependent $A(y_0, \Omega)$ and $B(y_0, \Omega)$ that reproduce the experimental forced vibration results have been identified; their values at six different amplitudes of forced vibration $y_0 = 0.2, 0.4...1.2$ are presented in Fig.B.16. Then, attempt has been made to determine the values of the coefficients in Eq.(B.1) by finding the best fit of the curves in Fig.B.16 with Eq.(B.2) using least-square method. We did not succeed in finding a good fit of the set of curves with polynomials given by Eq.(B.2); the fitting results are shown in Fig.B.16 and the associated values of the coefficients are $A_0 = 7.664, A_1 = 51.45, A_2 = -23.27, A_3 = 7.482, \tilde{A}_1 = -147.2, \tilde{A}_2 = 25.23, \hat{A} = 22.16, B_0 = 2.923, B_1 = 16.81, B_2 = -2.109, B_3 = -35.56, \tilde{B}_1 = -0.996, \tilde{B}_2 = 18.95, \hat{B} = -39.34$. Using these parameters, the forced vibration tests have been simulated and results are presented in Fig.B.17 in comparison with experimental results. It is clear from Fig.B.17 that the tuning of the model with additional velocity and acceleration dependent nonlinear couplings, as given by Eq.(B.2), using the approach described above does not produce a better agreement with the experimental results compared to the original amplitude dependent nonlinear couplings as shown in Fig.10. It has also been tried by the authors to tune the model manually. However, due to the complexity of the model, the model is difficult to be tuned and no significant improvement has been obtained.

[1] C. Williamson, R. Govardhan, Vortex-Induced Vibrations, Annu. Rev. Fluid Mech. 36 (1) (2004) 413–455.

[2] T. Sarpkaya, A critical review of the intrinsic nature of vortex-induced vibrations, J. Fluid Struct. 19 (4) (2004) 389–447.

[3] R. Gabbai, H. Benaroya, An overview of modeling and experiments of vortex-induced vibration of circular cylinders, J. Sound Vib. 282 (3) (2005) 575–616.

[4] R. Hartlen, I. Currie, Lift-Oscillator of Vortex-Induced Vibration, J. Eng. Mech. (EM5) (1970) 577–591.

[5] R. Skop, O. Griffin, A model for the vortex-excited resonant response of bluff cylinders, J. Sound Vib. 27 (2) (1973) 225–233.

[6] W. Iwan, R. Blevins, A Model for Vortex Induced Oscillation of Structures, J. Appl. Mech. 41 (1974) 581.

[7] R. Landl, A mathematical model for vortex-excited vibrations of bluff bodies, J. Sound Vib. 42 (2) (1975) 219–234.

[8] M. Facchinetti, E. de Langre, F. Biolley, Coupling of structure and wake oscillators in vortex-induced vibrations, J. Fluid Struct. 19 (2004) 123–140.

[9] N. Srinil, H. Zanganeh, Modelling of coupled cross-flow/in-line vortex-induced vibrations using double Duffing and van der Pol oscillators, Ocean Eng. 53 (Supplement C) (2012) 83–97.

[10] X. Bai, W. Qin, Using vortex strength wake oscillator in modelling of vortex induced vibrations in two degrees of freedom, Eur. J. Mech. B Fluids 48 (Supplement C) (2014) 165–173.

[11] A. Postnikov, E. Pavlovskaia, M. Wiercigroch, 2DOF CFD calibrated wake oscillator model to investigate vortex-induced vibrations, Int. J. Mech. Sci. 127 (Supplement C) (2017) 176–190, special Issue from International Conference on Engineering Vibration - ICoEV 2015.

[12] A. Farshidianfar, H. Zanganeh, A modified wake oscillator model for vortex-induced vibration of circular cylinders for a wide range of mass-damping ratio, J. Fluid Struct. 26 (3) (2010) 430 – 441.

[13] A. Farshidianfar, N. Dolatabadi, Modified higher-order wake oscillator model for vortex-induced vibration of circular cylinders, Acta Mech. 224 (7) (2013) 1441–1456.

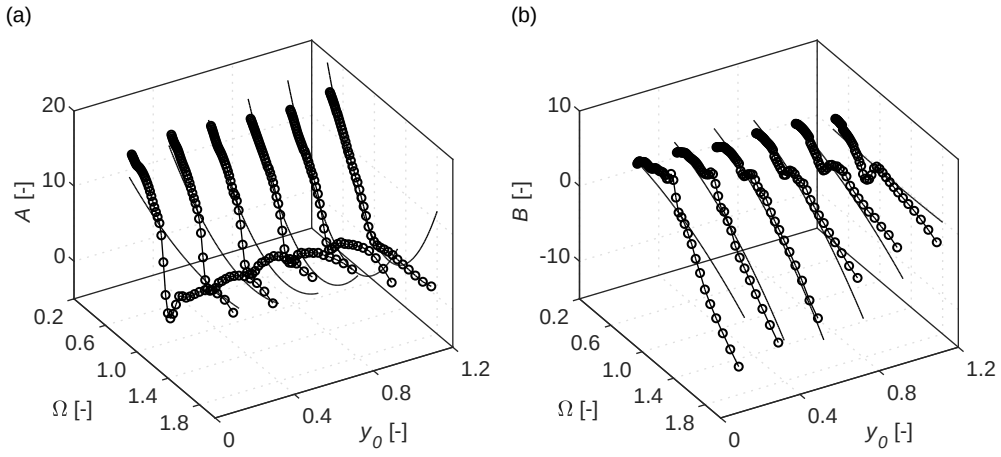

Figure B.16: Determined values of (a) $A(y_0, \Omega)$ and (b) $B(y_0, \Omega)$ as a function of amplitude and frequency of cylinder oscillation (marked by lines with circles), and curve fit (solid lines) found by least square method.

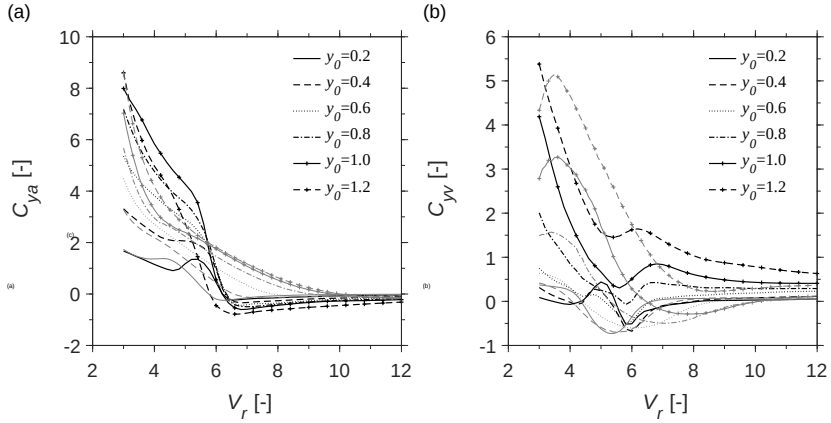

Figure B.17: A comparison of the wake oscillator model with additional velocity and acceleration dependent nonlinear couplings (gray thin lines) and the forced vibration measurements (black thick lines) for the force coefficient (a) in phase with acceleration C_{ya} and (b) in phase with velocity C_{yv}.

[14] V. Kurushina, E. Pavlovskaia, A. Postnikov, M. Wiercigroch, Calibration and comparison of VIV wake oscillator models for low mass ratio structures, Int. J. Mech. Sci. 142-143 (2018) 547 – 560.
[15] R. Ogink, A. Metrikine, A wake oscillator with frequency dependent coupling for the modeling of vortex-induced vibration, J. Sound Vib. 329 (2010) 5452–5473.
[16] A. H. P. van der Burgh, Nonlinear Dynamics of Structures Excited by Flows, in: D. Habault (Ed.), Fluid-Structure Interactions in Acoustics, chap. 6, Springer-Verlag Wien GmbH, 221–259, 1999.
[17] R. Skop, S. Balasubramanian, A New Twist on an Old Model For Vortex-Excited Vibrations, J. Fluid Struct. 11 (4) (1997) 395–412.
[18] T. Sarpkaya, In-Line And Transverse Forces On Cylinders In Oscillatory Flow At High Reynolds Numbers, J. Mar. Res. 21 (4) (1977) 200–216.
[19] L. Qin, Development of Reduced-Order Models for Lift and Drag on Oscillating Cylinders with Higher-Order Spectral Moments, Ph.D. thesis, Virginia Polytechnic Institute and State University, 2004.
[20] R. Gopalkrishnan, Vortex-induced forces on oscillating bluff cylinders, Ph.D. thesis, Woods Hole Oceanographic Inst., MA., 1993.
[21] C. Williamson, A. Roshko, Vortex formation in the wake of an oscillating cylinder, J. Fluid Struct. 2 (4) (1988) 355–381.
[22] A. Nayfeh, F. Owis, M. Hajj, A Model for the Coupled Lift and Drag on a Circular Cylinder, in: ASME International Design Engineering Technical Conferences, Computers and Information in Engineering Conference, 1289–1296, 2003.
[23] O. Marzouk, A. H. Nayfeh, I. Akhtar, H. N. Arafat, Modeling Steady-state and Transient Forces on a Cylinder, J. Vib Control. 13 (7) (2007) 1065–1091.
[24] A. Leonard, A. Roshko, Aspects of Flow-Induced Vibration, J. Fluid Struct. 15 (3) (2001) 415 – 425.
[25] A. Khalak, C. Williamson, Motions, Forces and Mode Transitions in Vortex-Induced Vibrations at Low Mass-Damping, J. Fluid Struct. 13 (7) (1999) 813–851.
[26] W. C. Elmore, M. A. Heald, Physics of Waves, Dover Publications, New York, 1989.
[27] B. Gustavsen, A. Semlyen, Rational approximation of frequency domain responses by vector fitting, IEEE Trans. Power Del. 14 (3) (1999) 1052–1061.